Evolution of the $N = 28$ shell closure: a test bench for nuclear forces

O. Sorlin[1] **and M.-G. Porquet**[2]

[1]Ganil, CEA/DSM-CNRS/IN2P3, B.P. 55027, F-14046 Caen Cedex 5, France
[2]CSNSM, CNRS/IN2P3 - Université Paris-Sud, F-91405 Orsay, France

E-mail: sorlin@ganil.fr,porquet@csnsm.in2p3.fr

Abstract. The evolution of the $N = 28$ shell closure is investigated far from stability. Using the latest results obtained from various experimental techniques, we discuss the main properties of the $N = 28$ isotones, as well as those of the $N = 27$ and $N = 29$ isotones. Experimental results are confronted to various theoretical predictions. These studies pinpoint the effects of several terms of the nucleon-nucleon interaction, such as the central, the spin-orbit, the tensor and the three-body force components, to account for the modification of the $N = 28$ shell gap and spin-orbit splittings. Analogies between the evolution of the $N = 28$ shell closure and other magic numbers originating from the spin-orbit interaction are proposed ($N = 14, 50, 82$ and 90). More generally, questions related to the evolution of nuclear forces towards the drip-line, in bubble nuclei, and for nuclei involved in the r-process nucleosynthesis are proposed and discussed.

PACS numbers: 21.10.-k, 21.30.-x, 21.60.-n, 27.30.+t, 27.40.+z

1. Introduction

Guided by the existence of a spin-orbit coupling in atomic physics, M. Goeppert Mayer [1] and O. Haxel *et al* [2] independently postulated in 1949 the existence of a strong spin-orbit (SO) force in the one-body nuclear potential to reproduce the so-called 'magic numbers' above 20. Their SO interaction has to be attractive for nucleons having their angular momentum aligned with respect to their spin (denoted as $\ell_\uparrow$) and repulsive in case of anti-alignment ($\ell_\downarrow$). Its strength was constrained to reproduce the size of the shell gaps at 28, 50, 82, and 126 derived from experimental data obtained in the early days of nuclear structure studies.

During the last two decades, major experimental and theoretical breakthroughs have strengthened that, though this simplified mean field picture of the SO interaction is elegant and simple, the observed SO splitting comes from the combination of complex effects due to the nuclear force. In particular, the size of the $N = 28$ shell gap is governed by the spin-orbit, the tensor, the three-body force components, and possibly the change of nuclear forces at the drip-line due to interactions with the continuum. For instance, the $N = 28$ shell gap grows by about 2.7 MeV between ^{41}Ca and ^{49}Ca to

reach a value of 4.8 MeV. This effect has recently been mainly inferred to three-body forces. Then, starting from the doubly-magic $^{48}_{20}Ca_{28}$ nucleus and removing protons, a progressive onset of deformation is found to occur: $^{46}_{18}Ar$ is a moderately collective vibrator, $^{44}_{16}S$ exhibits a prolate-spherical shape coexistence, the $^{42}_{14}Si$ nucleus is a well oblate nucleus, and the newly discovered $^{40}_{12}Mg$ is likely to be a prolate nucleus. Such a progressive change of structure is triggered by the combination of three effects: the reduction of the spherical $N = 28$ shell gap, the probable reduction of the $Z = 14$ sub-shell gap *and* the increase of quadrupole excitations across these gap, i.e. on the one side between the neutron $1f_{7/2}$ and $2p_{3/2}$ orbits and on the other side between the proton $1d_{5/2}$ and $2s_{1/2}$ orbits which are separated by two units of angular momenta ($2\hbar$).

This smooth but continuous change of nuclear shapes at the semi-magic $N = 28$ nuclei is quite unique in the chart of nuclides. Therefore from this study we can learn how a spherical rigid system could evolve towards a very collective system when a few nucleons are removed. There, proton-neutron forces act between nucleons in orbits which are different from the ones occupied in the valley of stability, hereby involving new facets of the nuclear forces which were not yet tested.

The magic number 28 is in fact the third number of nucleons which is created by the SO splitting‡, the first two SO gaps being 6 and 14. Similar components of the nuclear forces are expected to play a role in the gap values of all the SO magic numbers, leading to possibly similar consequences throughout the chart of nuclides. The magic number 28 is a target choice to study nuclear forces as it involves nuclei having an intermediate mass and size, with orbits relatively well separated from the neighboring ones. This feature is essential to distinguish the effects of nuclear forces between nucleons occupying orbits having different properties (such as the number of nodes, the angular momentum and the spin orientation). Conversely as the size of nuclei grows, the in-medium nuclear force is weaker and modification of shell structures occur only when many nucleons are involved. Added to this, the nuclear orbits are more compressed in energy and their occupancy is diluted by nucleon-pair scatterings. It follows that the action of specific nuclear forces between nucleons in well established orbits is much more difficult to disentangle in heavy than in light systems. At the other extreme, if the system is composed of a small number of nucleons, the change of only few nucleons leads to very rapid and drastic structural changes and the very concept of the mean-field approach becomes inappropriate. To quote one example of quick change of a SO magic gap, the $N = 14$ gap collapses already after the removal of two protons, from ^{22}O to ^{20}C.

On the experimental point of view, an incredible wealth of information has been obtained these last two decades by studying the evolution of nuclear structure south to the doubly-magic $^{48}_{20}Ca_{28}$ nucleus. Different experimental techniques are used worldwide, such as β or isomeric-decay studies, atomic mass measurements, Coulomb excitation, transfer reaction, or in-beam γ-ray spectroscopy. These studies became feasible since

‡ Note that from now on, we will rather explicitly mention SO *splitting* rather than SO *interaction* as the shell gaps are created by several components of the nuclear force, and not exclusively by the spin-orbit force.

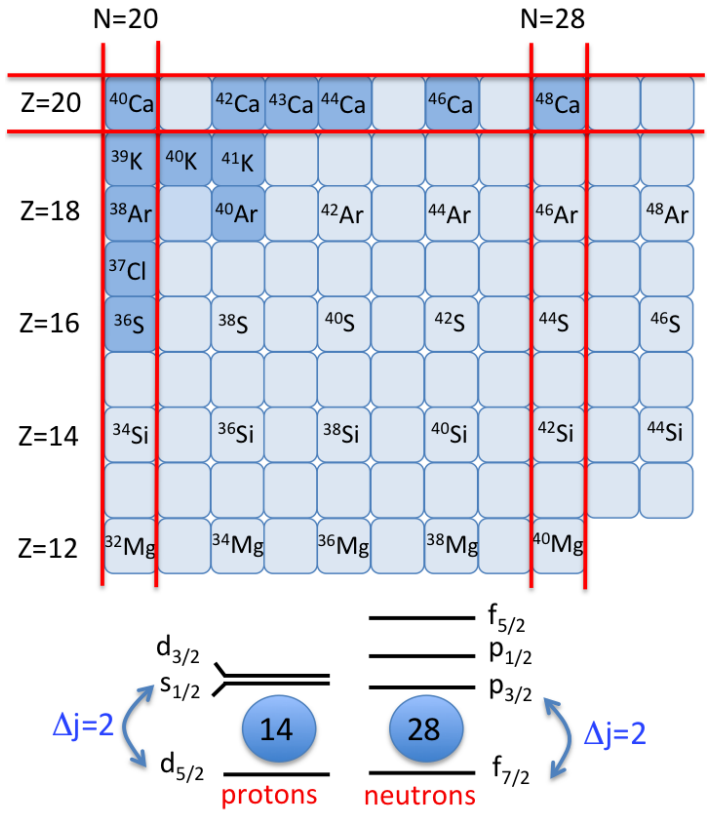

Figure 1. Part of the chart of the nuclides which will be considered in the present work. Stable nuclei are displayed with a dark blue color. In the bottom part, the orbits of the proton and neutron valence spaces under study are shown.

increasing beam intensities of ^{48}Ca and detectors capabilities become available. With 8 neutrons more than the most abundant ^{40}Ca isotope, the ^{48}Ca isotope represents a fraction about 0.2% of the total Ca isotopes on earth. However it is more than 50 times more abundant than the $(N-2)$ nucleus ^{46}Ca on earth, a feature which is not so common in the chart of nuclides. This is ascribed to its double magicity which makes it produced in significant amount and poorly destroyed in specific stellar explosive environments. In some sense, nature has offered with the neutron-rich and doubly magic ^{48}Ca isotope a rather unique tool to study the behavior of nuclear forces far from stability.

We shall explore in the next Sections the nuclear structure evolution of the nuclei presented in Figure 1. In Section 2, the general properties of atomic masses, first excited states and reduced transition probabilities will be presented. In Section 3, we shall discuss upon the evolution of proton orbits when moving from $N = 20$ to $N = 28$ by studying the odd-Z isotopic chains of $_{19}$K, $_{17}$Cl and $_{15}$P. Sections 4 and 5 show the evolution of the $N = 28$ gap from the behaviors of the $N = 27$ and $N = 29$ isotones. Some experimental and theoretical challenges related to the nuclear forces responsible for the SO magic numbers will be proposed in the last Section.

Sections 2 to 5 of the present paper update our previous work on the evolution of the $N = 28$ shell closure [3].

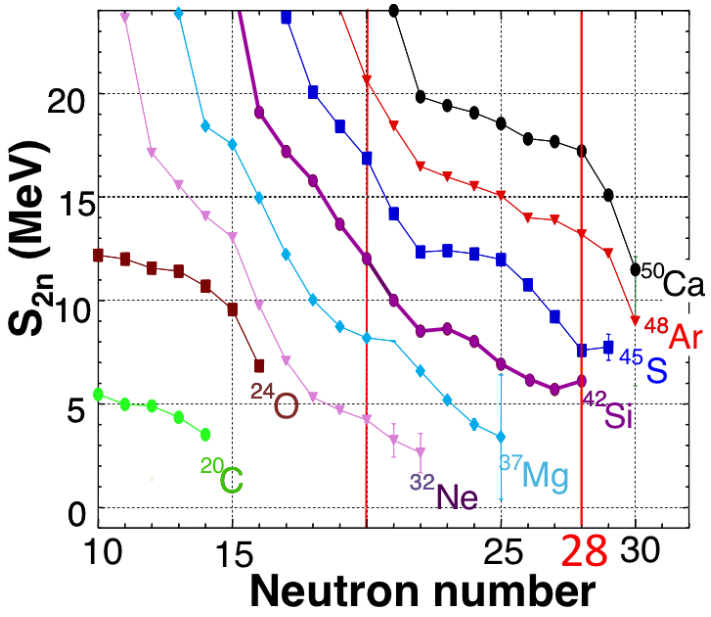

Figure 2. Evolution of the two-neutron separation energy S_{2n} in the even-Z isotopic chains (experimental atomic masses from Refs. [4, 5]). The sharp drop in S_{2n} observed in the Ca isotopic chain after $N = 28$ progressively disappears far from stability.

2. View of the shell-structure evolution from atomic masses, $E(2_1^+, 0_2^+, 4_1^+)$ and $B(E2; 0_1^+ \rightarrow 2_1^+)$ values

2.1. Atomic masses

The two-neutron separation energy $S_{2n}(A)$ can be obtained in a given isotopic chain from the atomic-mass differences between nuclei having A and $A-2$ nucleons. The trend of $S_{2n}(A)$ is in general rather smooth, except after having passed a major shell gap. There, when adding 2 more neutrons, the $S_{2n}(A)$ value drops significantly. This is an indication that a shell closure is efficient and that a spherical shell gap is existing. Such a sharp drop in $S_{2n}(A)$ is observed in the Ca and Ar isotopic chains (see Figure 2). On the other hand, the S and Si isotopic chains behave differently. An *increase* in $S_{2n}(A)$ is observed in the S chain when crossing $N = 28$ and in the Si chain, just before crossing $N = 28$. This indicates a clear deviation to sphericity at $N = 28$ in these isotopic chains. This increase of $S_{2n}(A)$ around $N = 28$ likely arises from the increase of binding energy due to correlations, which goes in concert with the onset of deformation. These hypotheses need to be confirmed with other nuclear properties such as the first 2_1^+ energy and the reduced transition probability $B(E2; 0_1^+ \rightarrow 2_1^+)$.

2.2. Evolution of $E(2_1^+)$ and $B(E2; 0_1^+ \rightarrow 2_1^+)$ values in the $N = 20 - 28$ nuclei

Most generally, magic (spherical) nuclei are characterized by high $E(2_1^+)$ and weak $B(E2; 0_1^+ \rightarrow 2_1^+)$ values. Any deviation from this trend reveals a change in nuclear structure. The systematics of the $E(2_1^+)$ and B(E2) values from ^{40}Ca to ^{48}Ca (see

Figure 3) is often used to model multi-particle configurations of valence nucleons in one particular orbit, which is the $\nu f_{7/2}$ orbit in the present case. In this framework, the 2_1^+ energies are maximum at the beginning of the shell ($N = 20$) where there is no valence neutron, and the end of the shell ($N = 28$) where neutron excitations can no longer occur in the same shell. The 2_1^+ energies are almost constant in between. In parallel the B(E2) values follow a bell-shape curve with minima at the two extremes of the shell according to the relation:

$$B(E2) \propto F(F-1) \tag{1}$$

where F is the fractional filling of the shell, which amounts here to $F = (N-20)/8$.

A deviation to this curve would be due to the breakdown of a spherical shell gap and an onset of deformation. Importantly, it could also happen when the configuration of the 2_1^+ state changes from a neutron origin to proton one in a given isotopic chain. In this case a sudden enhancement in $B(E2)$ value can be observed as protons carry a much larger effective charge than neutrons (typically e_p=1.5 while e_n=0.5). Added to the $E(2_1^+)$ and $B(E2)$ values, the 4_1^+ and 0_2^+ energies provide important complementary information on the evolution of the shell structure. The ratio $E(4_1^+/2_1^+)$ is often used as an indicator of deformation, while the location of the 0_2^+ state and the reduced electric monopole strength $\rho(E0; 0_2^+ \rightarrow 0_1^+)$ are used to probe shape coexistence.

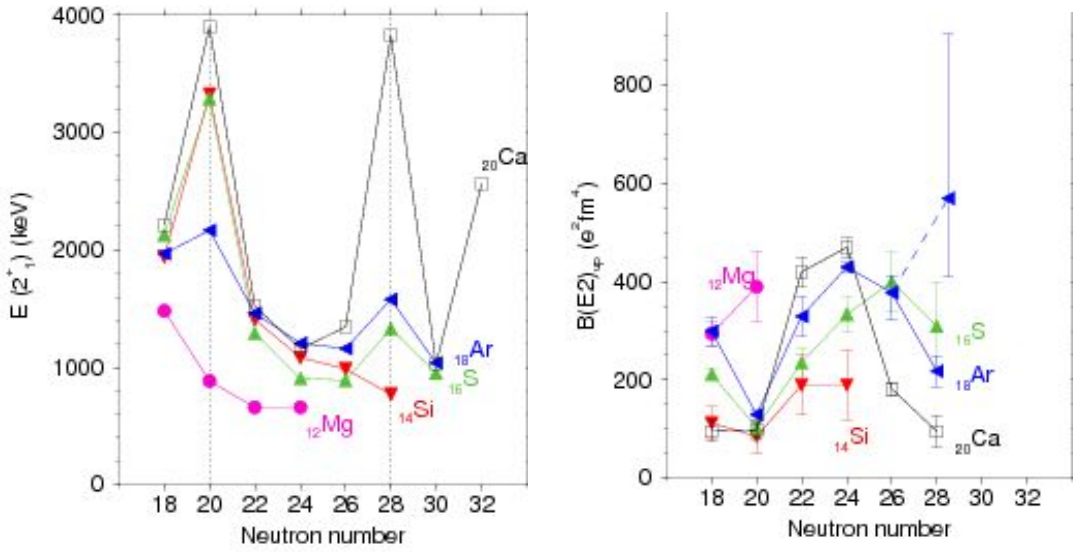

Figure 3. Experimental $E(2_1^+)$ energies (left) and $B(E2; 0_1^+ \rightarrow 2_1^+)$ values, also noted $B(E2)_{up}$ or $B(E2)\uparrow$, (right) in the $_{12}$Mg to $_{20}$Ca isotopic chains as a function of the neutron number N. Data are taken from the compilation of Ref. [6], except for ^{38}Si [7], ^{40}Si [8], ^{42}Si [9], ^{40}S [10], ^{46}S [11], ^{44}Ar [12], ^{46}Ar [13, 14], and ^{48}Ar [15].

Figure 3 shows the evolution of the 2_1^+ energies and of the reduced transition probabilities $B(E2; 0_1^+ \rightarrow 2_1^+)$ as a function of the neutron number in the $_{12}$Mg, $_{14}$Si, $_{16}$S, $_{18}$Ar and $_{20}$Ca isotopes. At $N = 20$, the 2^+ energies are high for all isotones, except

for $^{32}_{20}$Mg, in which a drop in energy is observed instead. The B(E2) values are small and remarkably similar for all $N = 20$ isotopes, except again for $^{32}_{20}$Mg. This picture is consistent with a strong shell closure $N = 20$ which persists from $Z = 20$ to $Z = 14$, and disappears below $Z = 14$ (see [16] for further discussions). On the other hand, the behavior of the $N = 28$ isotones is different. The rise in 2^+_1 energies observed at $Z = 16 - 18$ is more modest than at $N = 20$. In particular, the rise at $^{44}S_{28}$ is much smaller than at $^{36}S_{20}$. In $^{42}_{14}Si_{28}$ a drop is observed, at variance with what was observed in the $^{34}Si_{20}$ isotope. Combining this view of the 2^+ energy trend and the evolution of $S_{2n}(A)$, one can surmise that the $N = 28$ shell closure is progressively vanishing below Ca. The trend in $B(E2)$ nicely confirms this statement, as discussed in the next Section.

2.3. Spectroscopy of the even-Z $N = 28$ isotones

In this Section, we discuss more precisely some properties of the even-Z $N = 28$ isotones, from $Z = 18$ to $Z = 12$.

2.3.1. ^{46}**Ar** As the Ar isotopes have an open proton shell configuration, the 2^+_1 state is likely to be *mainly* of proton origin there. The 2^+_1 energy at the $N = 20$ and $N = 28$ shell closures is smaller in the Ar isotopes as it comes naturally from the proton recoupling inside the *sd* shells. However, a rise in 2^+ energy is found, witnessing the presence of neutron shell closures. It is worth noting that two very different values of $B(E2; 0^+_1 \rightarrow 2^+_1)$ values have been determined in ^{46}Ar (Figure 3). They arise from two different experimental techniques. On the one side, two experiments were carried at the NSCL facility to study the Coulomb excitation of ^{46}Ar. They led to consistent results, with a rather small $B(E2)_{up}$ value of 218(31) e^{2}fm^4 [13]. On the other side, a fairly large $B(E2)_{up}$ value of 570 $^{+335}_{-160}$ e^{2}fm^4 was deduced from another experiment performed at the Legnaro facility by Mengoni *et al* [14]. In this work, the ^{46}Ar was produced by means of multi-nucleon transfer reaction. The lifetime of the 2^+_1 state was determined by using the differential recoil distance Doppler shift method. In addition, a tentative 4^+_1 state has been proposed at 3892 keV by Dombrádi *et al* [17], leading to E($4^+_1/2^+_1$)=2.47, a value which lies between the limits of vibrator and rotor nuclei.

Comparison of these two $B(E2)$ values to models is very instructive. The recent relativistic Hartree-Bogoliubov model based on the DD-PC1 energy density functional [18] reproduces very well the low value of Ref. [13], while the Shell-Model (SM) calculations of Nowacki *et al* [19] agree with the large value of Ref. [14]. It therefore seems that, though only two protons below the doubly-magic ^{48}Ca nucleus, ^{46}Ar is still a challenging nucleus to modelize.

Interesting to add is the fact that the B(E2) in ^{47}Ar [20] is close to the lowest value measured in ^{46}Ar, i.e. at variance with the SM predictions, while the $B(E2)$ experimental result and SM calculations agree with an enhanced collectivity for ^{48}Ar [20]. SM calculations also account for the spectroscopy of higher energy states in ^{48}Ar obtained from deep-inelastic transfer reactions, which show that its deformation is

likely nonaxially symmetric [15]. To conclude, a new measurement of the B(E2) in ^{46}Ar is therefore called for to see if a local discrepancy between SM calculations and experimental results persists at $N = 28$.

2.3.2. **^{44}S** The $B(E2; 0_1^+ \rightarrow 2_1^+)$ and 2_1^+ energy values in ^{44}S, determined using Coulomb excitation at high energy at the NSCL facility by Glasmacher *et al* [21], point to a configuration which is intermediate between a spherical and deformed nucleus. Evidence of shape coexistence was found at GANIL by determining the decay rates of the isomeric 0_2^+ state at 1365(1) keV to the 2_1^+ at 1329(1) keV and 0_1^+ ground state through delayed electron and γ spectroscopy [22]. Comparisons to shell-model calculations point towards prolate-spherical shape coexistence. A schematic two-level mixing model was used to extract a weak mixing between the two configurations, the 0_1^+ state having a deformed configuration (i.e. a two-neutron particle-hole $2p2h$ excitation across the $N = 28$ spherical gap) and the 0_2^+ state, a spherical configuration (i.e. a zero-neutron particle-hole excitation $0p0h$). New excited states in ^{44}S were found afterwards [23, 24], which lend support to the shape coexistence hypothesis. By using the two-proton knockout reaction from ^{46}Ar at intermediate beam energy at NSCL, four new excited states were observed [23]. The authors proposed that one of them has a strongly deformed configuration, due to the promotion of a single neutron ($1p1h$) across the $N = 28$ gap. It would follow that three configurations would coexist in ^{44}S, corresponding to zero-, one-, and two-neutron particle-hole excitations. The one-proton knockout reaction from ^{45}Cl gave access to other excited states and their γ decays were measured using BaF_2 detectors at GANIL [24]. In particular the existence of the 2_2^+ state at 2156(49) keV is confirmed and is likely the expected 'spherical' 2^+ state. The Hartree-Bogoliubov model based on the DD-PC1 energy density functional [18] gives a relatively good agreement with experimental results, with the exception of a too large mixing between the 0_1^+ and 0_2^+ states. The Gogny force with the D1S set of parameters also gives a good description of ^{44}S, as described in Refs. [25, 26]. Shape coexistence has also been evidenced in the neighboring $^{43}S_{27}$ nucleus, which will be described in Section 4.

2.3.3. **^{42}Si** As to the $^{42}Si_{28}$ nucleus, Bastin *et al* [9] have established a 2^+ state at 770(19) keV. This experiment used nucleon removal reactions from secondary beams centered around ^{44}S at intermediate energy to produce the ^{42}Si nucleus and study the γ-rays from their de-excitation in flight. The detection of the γ-rays was achieved by arrays of detectors which surrounded the production target in which the reactions occurred. The dramatic decrease of the 2_1^+ energy in ^{42}Si is a proof of the disappearance of the spherical $N = 28$ shell closure at $Z = 14$. This extremely low energy of 770 keV -actually one of the smallest among nuclei having a similar atomic mass - cannot be obtained solely from neutron excitations. Proton-core excitations should play an important role, which could in principle be evidenced by measuring the evolution of the $B(E2)$ values in the Si isotopic chain while reaching $N = 28$. The $B(E2)$ values in the $_{14}$Si isotopic chain [27]

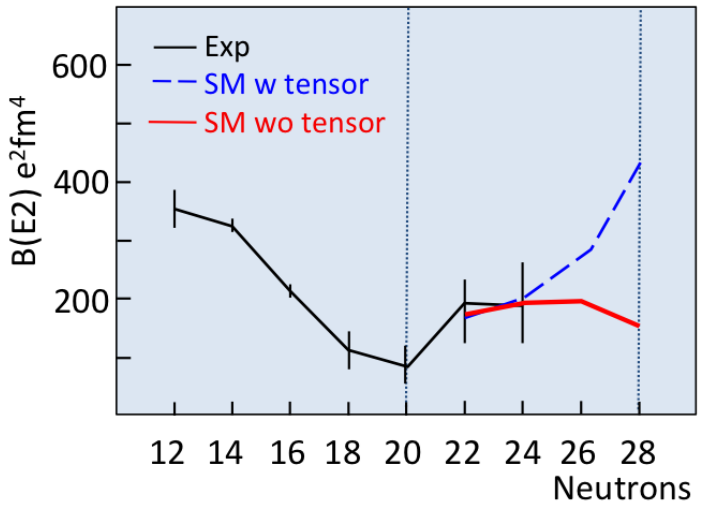

Figure 4. Evolution of the $B(E2)$ values in the Si isotopic chain. Experimental values are taken from Ref. [27] while theoretical values are taken from Shell-Model calculations using the sdpf-U interaction [19] in which monopole matrix elements contain tensor effects (dashed blue line) [28]. The result obtained when removing this tensor part is shown with a red line. The role of tensor forces is mainly seen at $N = 28$

seem to rise after $N = 20$, but not as much as in the $_{16}$S one (see the right part of Figure 3). Whether the $B(E2)$ values remain small, steadily increase up to $N = 28$, or follow a parabola cannot be judged at the present time as the quoted experimental error bars are too large. A reduced $Z = 14$ shell gap would dramatically increase the $B(E2)$ values, as protons are carrying most of the effective charge in the nucleus. The sole decrease of the $N = 28$ gap would barely change the 2_1^+ and $B(E2)$ values [9]. The effect of the tensor force is to reduce the 2_1^+ energy and enhance the $B(E2)$ value at $N = 28$ as shown in Figure 4, leading to $B(E2; 0_1^+ \rightarrow 2_1^+) \sim 430$ e^{2}fm^4 in ^{42}Si. Without implementing tensor parts in the monopole terms, the $B(E2)$ in ^{42}Si drops down to 150 e^{2}fm^4. One could deduce that the studies of the 2_1^+ state and the $B(E2)$ value in ^{42}Si are essential to ascertain the role of tensor forces at $N = 28$.

To conclude about the role of the tensor term in mean-field models, it requires a word of caution. Indeed, the B(E2) value of ^{42}Si has been calculated in the relativistic Hartree-Bogoliubov model of Li *et al* [18] and in the Gogny (D1S) model of Rodríguez-Guzmán *et al* [26]. These two models do not contain tensor force. However their B(E2) values differ significantly: 200 e^{2}fm^4 in [18] and about 470 e^{2}fm^4 in [26]. As far as the 2_1^+ energy is concerned, the value of Ref. [18] is twice as large as the experimental value, while the one of Ref. [26] is closer to experiment. Therefore the $B(E2)$ values should be measured and compared to theory in the *whole* Si isotopic chain to see if a significant increase is occurring at $N = 28$. The evolution of the *sd* proton orbits should be used as well as they influence strongly the B(E2) and E(2^+) values.

Further discussions on the implementation of tensor interaction and its role in the evolution of the gaps could be found for instance in Refs. [29, 30, 31, 32].

Results of a new experimental study of the excited states of ^{42}Si have just been published [33]. Thanks to the intense radioactive beams provided at RIKEN RIBF which enable $\gamma - \gamma$ coincidence measurements, the most probable candidate for the transition from the yrast 4^+ state to the 2^+ was identified, leading to a 4_1^+ energy of 2173(14) keV. Then the energy ratio, $R_{4/2} \sim 2.9$, corresponds to a well-deformed rotor. In addition, two other γ lines were measured at high energy (at 2032(9) and 2357(15) keV), which would deserve to be better characterized in order to assign other excited states of ^{42}Si.

2.3.4. ^{40}**Mg** Some years ago, the observation of three ^{40}Mg nuclei in the fragmentation of a primary beam of ^{48}Ca impinging a W target has ended the speculation about the location of the neutron drip-line at $Z = 12$ [34]. This isotope is predicted to lie inside the neutron drip line in many theoretical calculations (see for instance Ref. [35] and references therein). The relativistic Hartree-Bogoliubov model for triaxial nuclei was used to calculate the binding energy map of ^{40}Mg in the $\beta - \gamma$ plane [18], which predicts that this very neutron-rich isotope shows a deep prolate minimum at $(\beta, \gamma) = (0.45, 0^\circ)$. Shell model [19] as well as Gogny (D1S) [26] calculations predict an extremely prolate rotor as well. The identification of the first excited state of ^{40}Mg remains an ambitious challenge for the future. Conjectures about shell evolutions below ^{42}Si will be provided in Section 6.5.

3. Evolution of *sd* proton orbits as a function of the neutron number

3.1. The $\pi 2s_{1/2}$ and $\pi 1d_{3/2}$ orbits

The change of structural behavior between the $N = 20$ and $N = 28$ isotones can be partly ascribed to the evolution of the proton Single-Particle Energies SPE [36]. Using the pick-up reaction (d,^{3}He) from stable $_{20}$Ca targets, the evolution of the $\pi 2s_{1/2}$ and $\pi 2d_{3/2}$ spacing has been revealed in the $_{19}$K isotopic chain. The filling of eight neutrons in the $\nu 2f_{7/2}$ orbital induces an enhanced binding energy of the $\pi d_{3/2}$ orbit as compared to the $\pi 2s_{1/2}$ one. The spacing $\pi 2s_{1/2} - \pi 1d_{3/2}$ derived from SPE values drops from 2.52 MeV to -0.29 MeV, i.e. the orbits have crossed at $N = 28$. This is likely to be due to the fact that the monopole interaction $|V^{pn}_{1d_{3/2}1f_{7/2}}|$ is more attractive than the $|V^{pn}_{2s_{1/2}1f_{7/2}}|$ one. In Ref. [3] it was derived that

$$V^{pn}_{1d_{3/2}1f_{7/2}} - V^{pn}_{2s_{1/2}1f_{7/2}} \simeq -350\ keV. \quad (2)$$

The fact that $V^{pn}_{1d_{3/2}1f_{7/2}}$ is significantly more attractive than $V^{pn}_{2s_{1/2}1f_{7/2}}$ could qualitatively be ascribed to the fact that the proton $1d_{3/2}$ (ℓ=2, $\ell \downarrow$) and neutron $1f_{7/2}$ (ℓ=3, $\ell \uparrow$) wave functions have the same number of nodes and have attractive tensor terms as the proton and neutron spins are anti-aligned. On the other hand for $V^{pn}_{2s_{1/2}1f_{7/2}}$, the numbers of nodes differ and a large difference in the orbital momentum value is present between the two wave functions , making this monopole term weaker. Taking into account the monopole matrix elements solely, the evolution of $[E(1/2^+) - E(3/2^+)]$

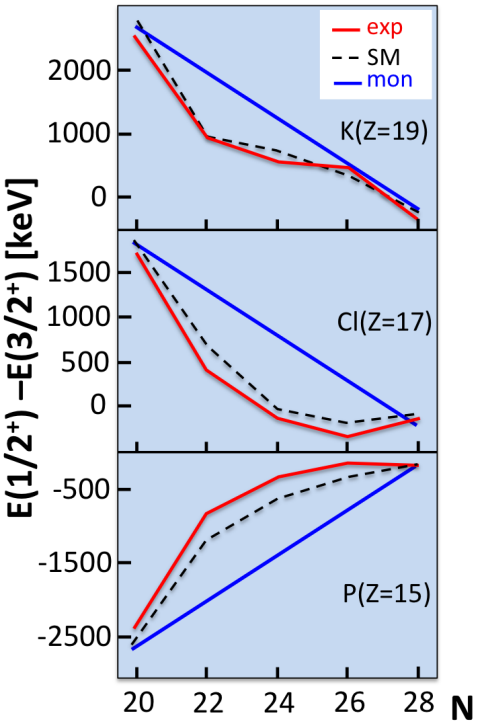

Figure 5. Calculated (black dashed line) and experimental (red line) values of $[E(1/2_1^+) - E(3/2_1^+)]$ along the K, Cl and P chains (adapted from Ref. [39]). The fixed monopole-driven trend (blue line) given by Equation 3 accounts well for the global evolution of $[E(1/2_1^+) - E(3/2_1^+)]$, while correlations are required at mid-shell. Note that for the P chain the ordering of the $1/2^+$ and $3/2^+$ states has changed as they correspond to particle states while they are hole states in the Cl and K chains.

between $N = 20$ and $N = 28$ would be linear as a function of the number of neutrons x leading to:

$$[E(1/2^+)-E(3/2^+)]_{20+x} = [E(1/2^+)-E(3/2^+)]_{20}+x(V^{pn}_{d_{3/2}f_{7/2}}-V^{pn}_{s_{1/2}f_{7/2}}) \quad (3)$$

The experimental evolution of $[E(1/2_1^+) - E(3/2_1^+)]$ deviates at mid shell from the linear monopole trend shown in Figure 5. This deviation is due to pairing and quadrupole correlations which already engage at $N = 22$, as soon as the single-particle states $\pi s_{1/2}$ and $\pi d_{3/2}$ come close enough to each other. Shell model calculations using the *sdpf* interaction [37] well reproduce these correlations [38, 39], as shown by the black dashed line in Figure 5.

The strong reduction between the proton $3/2^+$ and $1/2^+$ states is also found around $N = 28$ in the $_{17}$Cl and $_{15}$P isotopic chains. This demonstrates that the change in monopole interaction plays a decisive role in bringing the $\pi s_{1/2}$ and $\pi d_{3/2}$ states degenerate at $N = 28$. This has a profound consequence on the evolution of collectivity between $N = 20$, where a sub-shell gap exists between $\pi s_{1/2}$ and $\pi d_{3/2}$, and $N = 28$, where this sub-shell has vanished completely. As discussed above for the K isotopes, the evolution of the experimental $3/2_1^+$ and $1/2_1^+$ states for the Cl and P isotopes is distorted

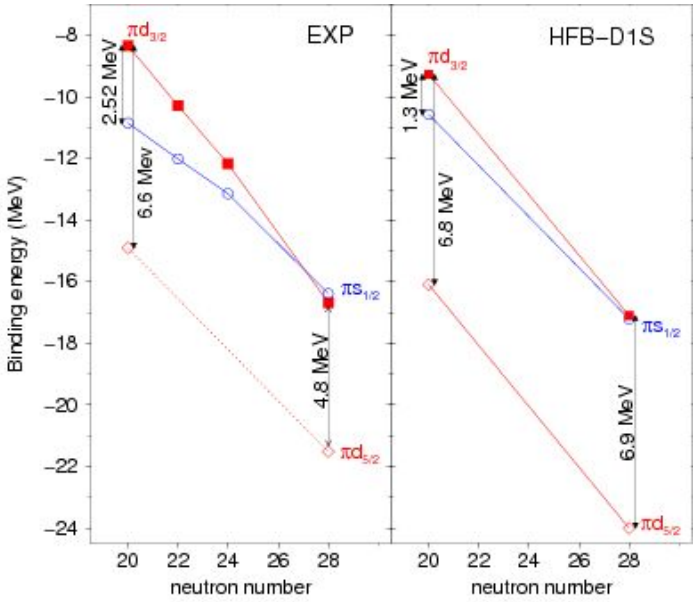

Figure 6. Left: Evolution of the proton $d_{5/2}$, $s_{1/2}$ and $d_{3/2}$ orbits in the K isotopic chain derived from experimental data. Right: Results of HFB calculations using the Gogny D1S interaction (see text).

by pairing and quadrupole correlations (see Figure 5), which are also well accounted for by shell-model calculations [39].

3.2. The $\pi d_{5/2}$ orbit

As shown before, the evolution of the $Z = 14$ shell gap is crucial for providing enhanced correlations in the $N = 28$ nuclei far from stability, as well as to probe the effect of tensor forces. However, as the single-particle strength is significantly spread in the ^{43}P nucleus, the size of the $Z = 14$ gap can hardly be extracted there from experimental data. In order to extract more accurately the change in the size of the $Z = 14$ gap when filling the neutron $f_{7/2}$ orbit from $N = 20$ to $N = 28$ we could in principle look at the evolution of the $s_{1/2}$ and $d_{5/2}$ single-particle energies in the K isotopic chain as deformation is not developing there.

However, one additional problem arises from the fact that in the K chain the $d_{5/2}$ orbit appears to be more bound by about 2.5 MeV than in the P isotopic chain. It follows that it is very hard to study the evolution of the $d_{5/2}$ single particle energy in the K chain as the $d_{5/2}$ strength is spread into many states which carry a small fraction of it (see the discussion in Section 4.2.3 of Ref. [3] and its Tables 2 and 3). With this important word of caution in mind, we can nevertheless discuss the evolution of the binding energies of the $\pi d_{5/2}$, $\pi s_{1/2}$ and $\pi d_{3/2}$ orbits between ^{39}K$_{20}$ and ^{47}K$_{28}$ in a semi quantitative way. The experimental part of Figure 6 displays a reduction of the proton $d_{5/2} - d_{3/2}$ splitting by about 1.7 MeV between $N = 20$ and $N = 28$. When adding neutrons in the $f_{7/2}$ shell, the two d orbits become more bound. This is mainly due to

the attractive proton-neutron interactions. The fact that the gain in binding energy is larger for the $1d_{3/2}$ orbit than for the $1d_{5/2}$ one comes from the fact that the $V^{pn}_{1d_{5/2}1f_{7/2}}$ monopole is weaker than $V^{pn}_{1d_{3/2}1f_{7/2}}$. It likely comes (at least partly) from the fact that $V^{pn}_{1d_{3/2}1f_{7/2}}$ ($V^{pn}_{1d_{5/2}1f_{7/2}}$) monopole contains an attractive (repulsive) tensor part as the proton and the neutron have anti-aligned (aligned) spin orientations.

Note that the size of the $Z = 14$ gap, which is almost similar for the two isotones ^{39}K and ^{35}P (the properties of ^{35}P are discussed in Section 3.4), is an essential ingredient for providing a similar structural behavior at $N = 20$ from ^{40}Ca to ^{34}Si.

3.3. Theoretical predictions of the evolution of the three orbits in the K isotopic chain

Interesting is to compare this variation of proton orbits to calculations obtained with Hartree-Fock (HF) self-consistent calculations using the D1S Gogny force [40, 41]. The binding energies of the single-particle levels of ^{40}Ca and ^{48}Ca have been obtained from HF calculations. As usual, the HF equations are firstly solved by iterative diagonalization of the HF Hamiltonian. Then the single-particle energies are defined as the eigenvalues of the self-consistent one-body Hamiltonian, obtained after convergence. In this approach, a change of the $s_{1/2} - d_{3/2}$ splitting is found from $N = 20$ to $N = 28$, but twice as small as experimentally. No change of the $d_{5/2} - d_{3/2}$ splitting is obtained (see the right part of Figure 6) as tensor interaction is not included. Moreover, as these orbits are well bound no reduction of the spin-orbit interaction associated with an extended surface density profile is foreseen. We conclude that a further reduction of the $d_{5/2} - d_{3/2}$ splitting is required to match the experimental results.

3.4. Comparison of $^{35}P_{20}$ and $^{43}P_{28}$

The development of collectivity in the $_{16}$S and $_{14}$Si isotopic chains depends on the amount of proton excitations across the $Z = 14$ gap, from the deeply bound proton $d_{5/2}$ to the degenerate $d_{3/2}$ and $s_{1/2}$ orbits (see the bottom part of Figure 1). When possible, the $s_{1/2}$-$d_{5/2}$ cross-shell excitations naturally bring quadrupole excitations. The comparative studies of the ^{35}P$_{20}$ and ^{43}P$_{28}$ nuclei gives valuable information on the reduction of the $Z = 14$ gap and the increasing role of correlations across it.

The energy of the three orbits, $\pi d_{5/2}$, $\pi s_{1/2}$ and $\pi d_{3/2}$, and their occupancy values, $(2J + 1) \times SF$ (where SF is the spectroscopic factor), have been obtained in ^{35}P$_{20}$ by Khan *et al* [42] by means of the ^{36}S$_{20}$(d,^{3}He)^{35}P$_{20}$ reaction. The major results are shown in the top part of Figure 7. The energy spectrum of ^{35}P$_{20}$ exhibits few levels, with rather large spacing. The sum of the occupancies of the two first states $s_{1/2}$ and $d_{3/2}$ is about 2, while most of the occupancy is in the $s_{1/2}$ orbit. As the $s_{1/2} - d_{3/2}$ spacing is not large enough (about 2.4 MeV) to smother pair scattering, some leak of occupancy from the $s_{1/2}$ to the upper $d_{3/2}$ orbit is present. The full $d_{5/2}$ strength is shared in three major fragments between 3.8 and 5.2 MeV excitation energy, leading to a mean value of the $Z = 14$ gap of 4.6 MeV. The picture is there rather simple, with

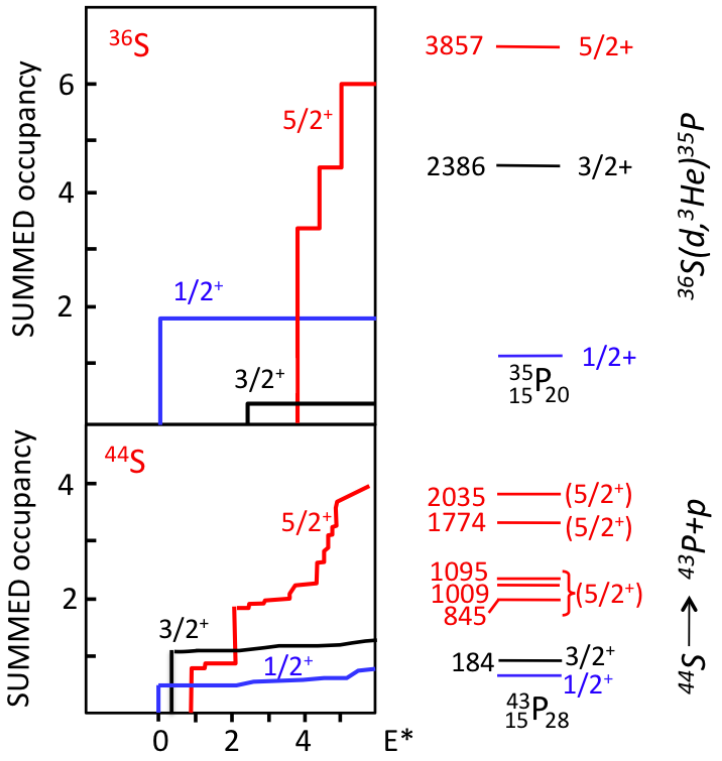

Figure 7. Top: Occupancy values of the proton $d_{5/2}$, $s_{1/2}$ and $d_{3/2}$ orbits are given for $^{35}P_{20}$. They were derived from spectroscopic factors obtained in the $^{36}S_{20}$(d,^{3}He)$^{35}P_{20}$ reaction [42]. The first excited states of $^{35}P_{20}$ are shown in the right part of the figure. Bottom (adapted from Ref. [43]): calculated occupancy values for $^{43}P_{28}$ derived from the $^{44}S_{28}$ (-1p) $^{43}P_{28}$ reaction. The level scheme of $^{43}P_{28}$ shown in the right part of the figure contains many $5/2^+$ states, witnessing a large spreading of the proton $d_{5/2}$ strength in this nucleus.

a sequence of $d_{5/2}$, $s_{1/2}$ and $d_{3/2}$ orbits bound by about 16.8 MeV, 12.2 and 9.8 MeV, respectively.

The situation gets more complex in the $^{43}P_{28}$ nucleus, which was studied by means of one proton knock-out reaction $^{44}S_{28}$ (-1p) $^{43}P_{28}$ by Riley *et al* [43]. At first glance it is clear in Figure 7 that the energy spectrum of $^{43}P_{28}$ is more compressed and contains many more levels than $^{35}P_{20}$ does. This compression of levels is relatively well reproduced by shell-model calculations using the interaction of Utsuno *et al* [44]. If the sum of the $s_{1/2}$ and $d_{3/2}$ occupancies still leads to about 2, the sharing of occupancy reflects the quasi degeneracy of these two orbits: since the $d_{3/2}$ orbits contains twice as many sub-states as the $s_{1/2}$ does its occupancy is implicitly twice as large. As to the $d_{5/2}$ strength, it is spread over many states among which only the ones below 2 MeV have been observed experimentally. Noteworthy is the fact that the $d_{5/2}$ strength already starts at low energy and a significant fraction is already calculated below 3 MeV. This high density of states at low energy as well as the spreading of the occupancy value are at variance with the picture observed in ^{35}P. In order to obtain a significant $d_{5/2}$ strength below 3.5 MeV in ^{43}P, the spherical $Z = 14$ gap has to be slightly reduced

between $N = 20$ and $N = 28$ [44, 9].

3.5. Summary

The development of collectivity in the neutron-rich $N = 28$ isotones is partly due to the reduction of the spacings between the protons $d_{5/2}$, $s_{1/2}$ and $d_{3/2}$ orbits as soon as the neutron $f_{7/2}$ orbit is completely filled. As these orbits are separated by 2 units of angular momentum, quadrupole (E2) collectivity is naturally favored. Added to this, a reduction of the $N = 28$ shell gap would reinforce this tendency to deform. Mean-field and shell-model theories agree on this description. We note that from the evolution of the proton *sd* orbits, mean-field theories need an additional spin-dependent term to reduce the $d_{5/2} - d_{3/2}$ splitting in order to match the experimental value.

It is important to note that a systematic study [45, 46] of the low-lying structures of many isotopic and isotonic chains was performed within the shell model approach, using the interaction of Nowacki and Poves [19]. In these works, a particular focus is also made on the cases with unpaired nucleons. Indeed the properties of the $N = 27$ and $N = 29$ isotones give a deeper understanding of the evolution of the $N = 28$ shell gap, as detailed in the two next Sections.

4. Structural evolution viewed from the $N = 27$ isotones.

The possible development of collectivity can be looked at in the $N = 27$ isotones, by comparing the characteristics of their first states. Shell-model calculations [45] have been performed by Gaudefroy *et al* using the interaction of Nowacki and Poves [19]. The results are drawn in Figure 8. In this plot, the configurations of the ground and the first excited states are displayed using a bi-dimentional representation, where the proton (neutron) configuration is shown on the y (x) axis. N_π (N_ν) gives the number of proton (neutron) *excitations* above the $0p0h$ ($0p1h$) core configuration and the size of the squares in the $N_\pi - N_\nu$ representation gives the intensity of each component.

About 90% of the g.s. configuration of the spherical ^{47}Ca nucleus corresponds to a neutron hole inside the $f_{7/2}$ shell ($0p1h$, N_ν=0) and a closed proton core ($0p0h$, N_π=0). The first-excited state with $I^\pi = 3/2^-$ at 2.02 MeV is expected to involve the promotion of one neutron in the upper $p_{3/2}$ shell with two neutron holes coupled in the $f_{7/2}$ shell ($1p2h$, N_ν=1). This is in agreement with the theoretical results showing that the first-excited state at 2.07 MeV corresponds mainly to the pure excitation of one neutron (N_ν=1) and to a minor extent, of three neutrons (N_ν=3). This state, with a closed proton configuration, would be found well above the ground state of all the $N = 27$ isotones, except if the $N = 28$ shell gap is reduced and correlations dominate.

The configurations of the g.s. and excited states in ^{45}Ar have been studied using ^{44}Ar(d,p)^{45}Ar [45] and ^{46}Ar(-1n)^{45}Ar [47] transfer and knock out reactions, respectively. Very good agreement is found between the experimental results, excitation energies and spectroscopic factors, and the theoretical predictions [45]. The drawings of Figure 8

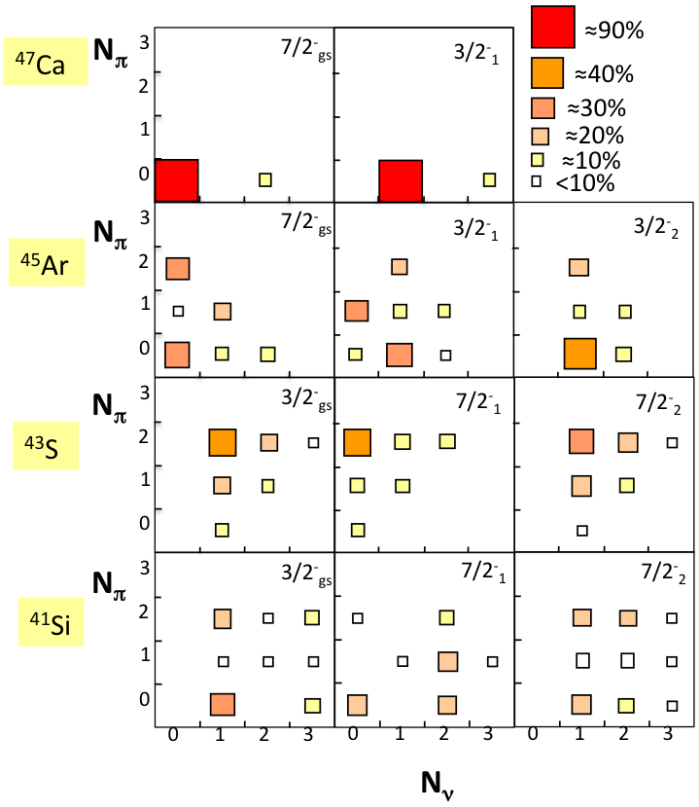

Figure 8. Squared wave functions of the first $7/2^-$ and $3/2^-$ states in the $N = 27$ isotones represented in the proton (N_π) versus neutron (N_ν) particle-hole configuration plane (see text for details), adapted from Ref. [45]. Some of the excitation energies are given in the text.

show that as compared to ^{47}Ca into which proton excitations are hampered by the $Z = 20$ gap, proton excitations are naturally present in ^{45}Ar inside the $s_{1/2}d_{3/2}$ proton states which are degenerate in energy at $N \sim 28$, as discussed in Section 3.1. These proton excitations occur as $1p1h$ ($N_\pi = 1$) or $2p2h$ ($N_\pi = 2$). They both contribute to the largest fraction of the $B(E2)$ values in the $Z = 16, 18$ nuclei. In line with these features the ^{45}Ar ground state is still dominated by a configuration similar to the one of ^{47}Ca, but correlations leads to a more mixed wave function. The state corresponding to the first-excited state in ^{47}Ca is more likely the second-excited state in ^{45}Ar ($3/2^-_2$) observed at 1.42 MeV and predicted at 1.22 MeV, for which the N_ν=0 component does not exist either. The configuration of the ($3/2^-_1$) state at 550 keV is in between the $7/2^-_{gs}$ and the $3/2^-_2$ configuration, which already witnesses the sharing of the p strength among several states.

Below ^{45}Ar, an inversion between the $7/2^-$ and $3/2^-$ states is predicted (see Figure 8). An isomer has been discovered in ^{43}S by Sarazin *et al* at 320 keV [48]. It was interpreted with the help of SM calculation to have a $7/2^-$ spin value and to decay to the $3/2^-$ ground state by a delayed transition. More recently, the g factor of this isomer was measured [49] establishing its spin-parity values, $I^\pi = 7/2^-$, and

implying a rather spherical shape for this state. Nevertheless, the value of its quadrupole moment is larger than expected for a single-particle state [50], implying that it contains non-negligible correlations that drive the state away from a purely spherical shape, in agreement with SM calculations (see Figure 8). In addition, an intermediate-energy single-neutron knockout reaction was used to characterize other excited states of ^{43}S [51]. Two of them are proposed to be members of the rotational band built on the deformed $3/2^-$ ground state, strengthening the case for shape coexistence in ^{43}S.

Note that this inversion of the $7/2^-$ and $3/2^-$ states, and the spreading of the wave function among neutron and proton excitations is, according to SM calculations, persisting in the $^{41}Si_{27}$ isotope. The spectroscopy of ^{39,41}Si has been carried out by Sohler *et al* [52] using the in-beam γ-ray spectroscopy method from few nucleon knockout reactions. The observation of low lying states in ^{39}Si call for a reduction of the $N = 28$ and $Z = 14$ shell gaps which induce the lowering of the intruder neutron $3/2^-$ state while going from $Z = 20$ to $Z = 14$. The energy of the only γ line, 672(14) keV, observed in ^{41}Si is significantly lower than the one of the first excited state in ^{47}Ca (2014 keV) suggesting a deformed ground state for ^{41}Si. However, as compared to shell-model predictions, some states expected at low energy have not been observed in ^{41}Si. It was suggested in Ref. [52] that a low-energy isomer would be present there. As isomers could not be evidenced with in-beam spectroscopy, another technique has to be used to reveal its existence. The search for this isomer and/or low-energy states would bring important pieces of information to confront to SM description. In Figure 8 one can observe that for ^{41}Si many squares have equal size, pointing to large mixing of proton and neutron configurations.

As mentioned above, the inversion between the natural $(\nu f_{7/2})^{-1}$ and the intruder $(\nu p_{3/2})^{+1}$ configurations of the ground states of the $N = 27$ isotones occurs between ^{45}Ar and ^{43}S. The properties of the ground state of ^{44}Cl therefore allow us to delineate the exact location of the inversion. This odd-odd nucleus has been populated by using the single neutron-knockout reaction from $^{45}Cl_{28}$ at intermediate beam energies at MSU [53]. The momentum distribution of the recoiling ^{44}Cl nuclei was analyzed for the direct population of its ground state, the best fit being obtained for the removal of an $\ell = 1$ neutron. This means that (i) there is a significant $(\nu p_{3/2})^{+2}$ component in the ground state of ^{45}Cl and (ii) this neutron orbit is involved in the ground state of ^{44}Cl. Therefore the intrusion of the $\nu p_{3/2}$ orbit from above the $N = 28$ shell closure occurs already for $Z = 17$. This is confirmed by the value of the g factor of the ground state of ^{44}Cl. This measurement, done at the LISE fragment separator at Ganil using the β nuclear magnetic resonance technique [54], indicates that $g(^{44}\mathrm{Cl})$ is significantly lower than $g(^{46}\mathrm{K})$. The two g values are well reproduced by SM calculations. While the main configuration of the ground state of ^{46}K is dominated by the spherical $(\pi d_{3/2})^3(\nu f_{7/2})^7$ configuration, the wave function of the ground state of ^{44}Cl is very fragmented, its second most-intense component, $(\pi s_{1/2})^1(\nu p_{3/2})^1$, explaining why the g factor of ^{44}Cl is reduced [54].

5. Structural evolution viewed from the $N = 29$ isotones.

In the previous sections, the erosion of the $N = 28$ shell gap below the doubly magic $^{48}_{20}$Ca has been probed through properties of atomic masses, energies of excited states and reduced transition probabilities, as well as through the spectroscopy of $N = 27$ isotones. The most direct way to evidence this erosion is to determine the evolution of the single particle energies between the $^{49}_{20}$Ca and $^{47}_{18}$Ar isotones. The study of ^{47}Ar$_{29}$ has been carried out by the $^{46}_{18}$Ar(d,p) transfer reaction in inverse kinematics at the GANIL/SPIRAL1 facility [55]. The obtained results were used to investigate the change of the $N = 28$ gap from $_{20}$Ca to $_{18}$Ar. From the Q value of the transfer reaction, the $N = 28$ gap was found to be of 4.47(9) MeV in ^{46}Ar, which is 330(90) keV smaller than in ^{48}Ca. Transfer to excited states were used to determine the energies and spectroscopic factors of the neutron $p_{3/2}$, $p_{1/2}$ and $f_{5/2}$ states in $^{47}_{18}$Ar. The fact that only part (about 3/4) of the strength for these states has been observed indicates that some correlations takes place already in ^{46}Ar, after the removal of only 2 protons from the doubly magic ^{48}Ca nucleus. In particular it was found in Ref. [55] that the $p_{3/2}$ orbit is already partially occupied through $1p-1h$ excitation across the $N = 28$ gap, from the $f_{7/2}$ orbit. The agreement between experiment results and SM calculations was rather good using the monopole terms of the *sdpf* [37] interaction. They were however slightly adjusted to match existing experimental data in this mass region [56]. By applying this technique, the full particle strength of the neutron $f_{7/2}$, $p_{3/2}$ and $p_{1/2}$ and $f_{5/2}$ orbits has been determined in ^{47}Ar. The resulting SPE are compared to those of the $^{49}_{20}$Ca isotone [57, 58] in Figure 9. It is found that from ^{47}Ar to ^{49}Ca the orbits in which the angular momentum is aligned with the intrinsic spin ($\ell_\uparrow$), such as $f_{7/2}$ and $p_{3/2}$, become relatively more bound than the $f_{5/2}$ and $p_{1/2}$ orbits where the angular momentum and intrinsic spin are anti-aligned ($\ell_\downarrow$). In particular, one can see in Figure 9 the asymmetry in gain of binding energy between the $f_{7/2}$ and $f_{5/2}$ orbits.

Bearing in mind that the $d_{3/2}$ and $s_{1/2}$ orbitals are quasi-degenerate at $N = 28$, (see Section 3.1), the addition of 2 protons between ^{47}Ar and ^{49}Ca occurs in an equiprobable manner§ in these orbits (i.e 1.33 in $1d_{3/2}$ and 0.66 in $2s_{1/2}$). Therefore modifications of neutron SPE arise from proton-neutron interactions involving these two orbits [55] and the change of the $N = 28$ shell gap (δG) can be approximated to :

$$\delta G^{pn}(28) \simeq 1.33(V^{pn}_{1d_{3/2}2p_{3/2}} - V^{pn}_{1d_{3/2}1f_{7/2}}) + 0.66(V^{pn}_{2s_{1/2}2p_{3/2}} - V^{pn}_{2s_{1/2}1f_{7/2}}) \quad (4)$$

Similarly, changes in the p and f SO splitting express as:

$$\delta SO = 1.33(V^{pn}_{1d_{3/2}\ell_\downarrow} - V^{pn}_{1d_{3/2}\ell_\uparrow}) + 0.66(V^{pn}_{2s_{1/2}\ell_\downarrow} - V^{pn}_{2s_{1/2}\ell_\uparrow}) \quad (5)$$

As regards the f states, the experimental change in SO splitting $\delta SO(f)$ was ascribed in [55] to the fact that the monopoles contain attractive and repulsive spin-dependent terms (which could be tensor terms) :

$$\delta SO(f) \simeq 1.33(V^{pn}_{1d_{3/2}1f_{5/2}} - V^{pn}_{1d_{3/2}1f_{7/2}}) \quad (6)$$

§ When taking into account the correlations expected in non doubly-magic nuclei, the occupation rates of the orbits are slightly modified, see for instance the numbers given in Ref. [56]

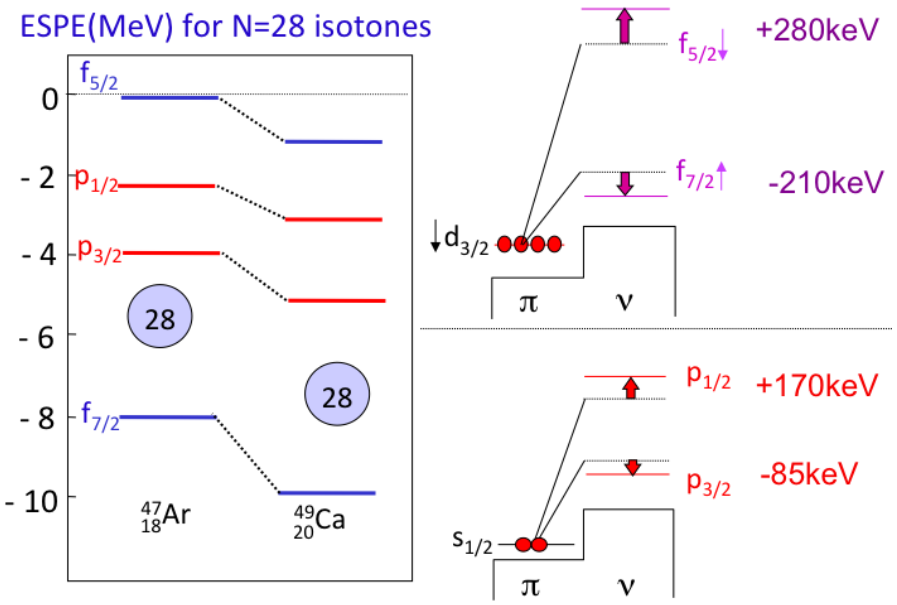

Figure 9. Left: Neutron single-particle energies (SPE) of the fp orbitals for the $^{47}_{18}\mathrm{Ar}_{29}$ and $^{49}_{20}\mathrm{Ca}_{29}$ nuclei. Right: Schematic view of the proton-neutron spin-dependent interactions involved to change the f (top) and p (bottom) SO splittings derived from the experimental data on ^{47}Ar in Refs. [55, 56].

As shown in Figure 9 the spin-dependent parts of the monopoles $\tilde{V}$ amount to $\tilde{V}^{pn}_{1d_{3/2}\ 1f_{7/2}}$ =-210 keV and $\tilde{V}^{pn}_{1d_{3/2}\ 1f_{5/2}}$=+280 keV, respectively. They amount to about 20% of the total monopole term $V^{pn}_{1d\ 1f}$. The change of the p SO splitting $\delta SO(p)$ was principally assigned in [56] to the removal of a certain fraction of $2s_{1/2}$ protons which depletes the central density‖ of the nucleus:

$$\delta SO(p) \simeq 0.66(V^{pn}_{2s_{1/2}2p_{1/2}} - V^{pn}_{2s_{1/2}2p_{3/2}}) \tag{7}$$

As shown in Figure 9, the corresponding spin-dependent part of the monopole terms was extracted to be of +170 keV and -85 keV for $\tilde{V}^{pn}_{s_{1/2}\ p_{1/2}}$ and $\tilde{V}^{pn}_{2s_{1/2}\ 2p_{3/2}}$, respectively.

The variation of the single-particle energies in terms of monopole interactions could be pursued towards the $^{43}_{14}$Si nucleus in which, as compared to $^{49}_{20}$Ca, *about* 4 protons have been removed in the $d_{3/2}$ and 2 in the $s_{1/2}$ orbits. We note here that protons are partly removed in the $d_{5/2}$ orbit as well. Using the monopole matrix elements derived in the interaction, changes in the spacing of the fp orbits is foreseen when the $d_{3/2}$ and $s_{1/2}$ orbits are empty. This leads to reductions of (i) the $N = 28$ gap by $0.33 \times 3 \simeq 1$ MeV, (ii) the f SO splitting by $\simeq 4(0.28 + 0.21) \simeq 2$ MeV and (iii) the p SO splitting by $\simeq 2(0.17 + 0.085) \simeq 0.5$ MeV. These global reductions are expected to reinforce

‖ Having an angular momentum ℓ=0, the $s_{1/2}$ orbit is peaked in the center of the nucleus. When no proton occupies the $s_{1/2}$ orbit, the central density is therefore depleted as compared to nuclei in which this orbit is filled. This property will be used in Section 6.3 to study the density dependence of the SO interaction.

particle-hole excitations across $N = 28$, which are of quadrupole nature.

It is important to note that, in the shell-model approach, the monopole terms do not vary when approaching the drip-line. Therefore when reaching the continuum the present approach and the concepts that have been used will be inappropriate. The proximity of continuum could already modify the binding energy of the $f_{5/2}$ orbit in ^{47}Ar, hereby possibly altering the role of tensor interaction derived from the present experimental data. The role of continuum should be quantified in this region.

6. Questions and perspectives

6.1. Introduction

As described in the previous sections, a wealth of spectroscopic information has been obtained from the study of the $N \simeq 28$ nuclei from $Z = 20$ down to $Z = 12$. Several important questions related to nuclear forces arose from these studies. In the following we propose to address some of them:

- What is the role of the three-body forces in providing the SO shell gaps ? Is there a general picture that is present throughout the chart of nuclides ?
- Can we disentangle the respective roles of the tensor and the spin-orbit components to account for the disappearance of $N = 28$ far from stability? Can we better understand the spin-orbit force ?
- Would other SO magic numbers (14, 50, 82 and 126) be disappearing far from stability as $N = 28$ does and if not why ?
- Which forces come into play in nuclei located below ^{42}Si, ^{78}Ni and ^{132}Sn?
- Are proton-neutron forces significantly modified when approaching the drip-line ?

We propose to discuss these questions using rather qualitative and phenomenological arguments based on experiments results.

6.2. What is the role of the three-body forces in providing the SO shell gaps ?

6.2.1. **Introduction** In this Section we investigate the role of neutron-neutron interactions to create the neutron SO shell gaps. The three-body forces are needed to create these gaps, which would not be obtained if realistic two-body forces would be used exclusively. We start with the study of the $N = 28$ shell gap and generalize this study to other SO shell gaps as $N = 14$, $N = 50$ and $N = 90$. We conclude that the three-body forces seem to play a similar and essential role to create the major shell gaps that leads to SO magic nuclei. We propose an empirical rule to predict the evolution of high-j orbits in superheavy nuclei as well as to create a sub-shell gap at $N = 90$, which could be of importance for the r-process nucleosynthesis.

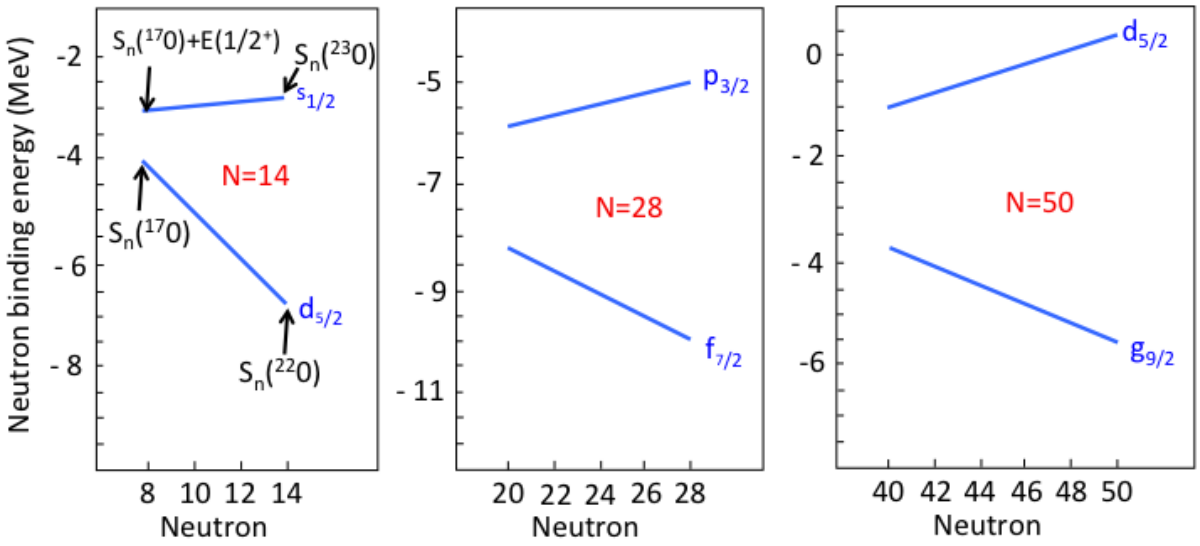

Figure 10. Evolution of neutron binding energies in the O (left), Ca (middle) and Ni (right) isotopic series. In each chain, the value of the neutron shell gap grows when adding neutrons in the high-j orbit ($d_{5/2}, f_{7/2}, g_{9/2}$ respectively). In the cases of the O and Ca chains, experimental values are taken at the two extremes of the binding energy values and a straight line is drawn in between, according to the monopole-driven trend. As for the Ni chain, details are found in the text.

6.2.2. **Neutron-neutron forces to create the $N = 28$ shell gap in Ca** Search for fp single-particle have been carried out using transfer reactions [59, 58] at $N = 20$ and $N = 28$ by studying the particle and hole strengths around the ^{40}Ca and ^{48}Ca nuclei, respectively. These experiments show that the $N = 28$ shell gap strongly increases when *adding neutrons* into the $f_{7/2}$ orbit, as the neutron $f_{7/2}$ ($p_{3/2}$) orbit gains (looses) binding energy. The gain in energy of the $N = 28$ gap from $N = 20$ to $N = 28$ is about $\delta G^{nn}(28) = 3$ MeV (see the middle of Figure 10). The mechanism which creates the large $N = 28$ shell gap, between the $f_{7/2}$ and $p_{3/2}$ orbits, is likely due to a strongly attractive $V^{nn}_{f_{7/2}\ f_{7/2}}$ and a repulsive $V^{nn}_{f_{7/2}\ p_{3/2}}$ monopole term¶. The increase of the $N = 28$ shell gap, $\delta G^{nn}(28)$, due to the neutron-neutron interactions can be written as a function of x (the number of neutrons added in the $f_{7/2}$ orbit) as :

$$\delta G^{nn}(28) = x[V^{nn}_{f_{7/2}p_{3/2}}] - (x-1)[V^{nn}_{f_{7/2}f_{7/2}}] \tag{8}$$

We note that the $(x - 1)$ term applies when neutrons occupy the same shell.

Effective two-body interactions derived from *realistic* interactions could not account for this increase of the $N = 28$ gap. For instance, it has been recently shown by Holt *et al* [60] that the $N = 28$ gap is almost constant using two-body forces and grows when three-body forces are taken into account. A more recent work which uses interactions from chiral effective field theory, leads to the same conclusion: the three-nucleon forces

¶ We note here that the V^{nn} are *effective* monopole terms. Even though they are written in a two-body form, they may contain three-body components.

create a $N = 28$ magic number [61] and generate the shell closure in ^{48}Ca. More generally it was proposed by Zuker [62] that the implementation of a three-body force can solve several deficiencies in nuclear structure.

6.2.3. **Neutron-neutron forces to create the $N = 14$ sub-shell gap in O** The $N = 14$ subshell gap, which is located between the $d_{5/2}$ and $s_{1/2}$ orbits, also comes from the SO splitting and shares similar properties as the $N = 28$ one. As shown in Figure 10, it grows by about $\delta G^{nn}(14)$=2.7 MeV from ^{17}O to ^{23}O as the neutron $d_{5/2}$ orbit is filled. Similar to the $N = 28$ gap, Equation 8 applies and the large value of the $N = 14$ gap at $N = 14$ is due to the strongly attractive (repulsive) $V^{nn}_{d_{5/2}\ d_{5/2}}$ ($V^{nn}_{d_{5/2}\ s_{1/2}}$) monopoles terms.

6.2.4. **Could we predict the size of the $N = 50$ shell gap in Ni?** From a phenomenological point of view, we can reasonably expect that a similar increase in binding energy of major shells having ℓ and s values aligned $\ell \uparrow$, i.e. $d_{5/2}$, $f_{7/2}$, $g_{9/2}$, $h_{11/2}$, will be occurring during their filling. This generally leads to an increase of shell gap by:

$$\delta G^{nn}(SO) = x[V^{nn}_{\ell_\uparrow(\ell-2)_\uparrow}] - (x-1)[V^{nn}_{\ell_\uparrow\ell_\uparrow}] \tag{9}$$

In particular, we could look at what is expected for the $N = 50$ shell gap from ^{68}Ni to ^{78}Ni, where fewer experimental data are available so far. Based on Equation 9 the gap formed between the $g_{9/2}$ and $d_{5/2}$ orbits is expected to grow as the $1g_{9/2}$ orbit is filled. The relevant effective monopole terms ($V^{nn}_{g_{9/2}\ g_{9/2}} \simeq$ -200 keV and $V^{nn}_{g_{9/2}\ d_{5/2}} \simeq$+130 keV) can be extracted from the spectroscopy of ^{88,90}Zr (see Figure 6 of Ref. [3]). When renormalizing the monopole terms to $A \simeq 75$ (using the hypothesis that V scales with $A^{-1/3}$) we find that the $N = 50$ gap should increase by about 3.1 MeV between $N = 40$ and $N = 50$. The right-hand side of Figure 10 displays the tentative change of the $N = 50$ gap in the Ni isotopic chain. The S_n value of ^{69}Ni as well as the *preliminary* energy of the $2d_{5/2}$ state at $\simeq$ 2.6 MeV derived from Ref. [63] are used. Note that a correction in binding energy is applied to $S_n(^{69}\text{Ni})$. Indeed it is likely that the $^{68}\text{Ni}_{40}$ ground state has a mixed contribution with the 0^+_2 state at 1.77 MeV. Taking a mixing of $50\%(\nu g_{9/2})^2 + 50\%(\nu p_{1/2})^{2+}$, it implies that before mixing the $(p_{1/2})^2$ configuration of ^{68}Ni is likely less bound by about 0.9 MeV. Thus starting from 2.6 MeV in ^{69}Ni, the $N = 50$ shell gap would reach (2.6+3.1=) 5.8 MeV in ^{78}Ni. This is somehow larger than what extrapolated from the $N = 50$ trend of binding energies [64] and with the SM predictions of Ref. [65]. Note that a small change in one of the V^{nn} values given above can drastically impact the value of the increased gap, as 10 neutrons (x =10) are involved here between $N = 40$ and $N = 50$ (see Equation 9).

If this later increase of shell gap is confirmed, this will remarkably show that similar forces (including the three-body term) are at play in the various regions of the chart

[+] This hypothesis comes from the comparison with experimental results obtained for $^{90}_{40}$Zr, showing that the configurations of its ground state and its 0^+_2 state at 1.76 MeV are $50\%(\pi g_{9/2})^2 + 50\%(\pi p_{1/2})^2$.

of nuclides to produce such large SO shell gaps. Even more *a priori* surprising is the increase of all the $N = 14$, $N = 28$ and $N = 50$ shell gaps by a *similar* value of about 3 MeV. This comes from the fact that two competing terms are involved to enlarge the gap in Equation 9. The two monopoles decrease with $A^{-1/3}$ as the nucleus grows in size, but they are multiplied by the number of neutrons x in the $\ell \uparrow$ orbit, which increases between $N = 14$ ($x = 6$ in $d_{5/2}$), $N = 28$ ($x = 8$ in $f_{7/2}$), and $N = 50$ ($x = 10$ in $g_{9/2}$). We could tentatively propose as an empirical rule that, during the filling of the $\ell \uparrow$ orbit, the variation of the major shell gaps of SO origin amounts to about 3 MeV. Though rather crude, this empirical rule could be used to predict the evolution of the $(j \uparrow, (j-2) \uparrow)$ orbits as a function of the filling of the $j \uparrow$ orbit. However, the pairing effect will dilute the orbital occupancy in heavier systems, as mentioned below for the $A = 132$ region of mass.

6.2.5. **Evolution of the $N = 82$ shell gap in Sn** As for the next shell $N = 82$, we probably expect the same increase of the $h_{11/2} - f_{7/2}$ spacing while filling the $h_{11/2}$ orbit. However this increase of gap could hardly be evidenced experimentally as the $h_{11/2}$ orbit is located close to two low-ℓ orbits, $s_{1/2}$ and $d_{3/2}$. So the pairing correlations dilute the occupancy of the high-j orbit with the two others, implying that the $h_{11/2}$ orbit is gradually filling when adding 18 neutrons from $N = 65$ to $N = 82$. Consequently the corresponding evolution of the $h_{11/2}$ binding energy is not only governed by the attractive $V^{nn}_{h_{11/2}\ h_{11/2}}$ interaction, but also by the repulsive ones, $V^{nn}_{h_{11/2}\ s_{1/2}}$ and $V^{nn}_{h_{11/2}\ d_{3/2}}$. Therefore, in this case, the SO empirical rule could be used as a guidance to constraint the spacing between the $\ell \uparrow$ and $(\ell - 2) \uparrow$ orbits at the mean-field level, *before* taking the role of correlations into account. It is important to point out that none of the self-consistent calculations reproduce the experimental location of the $\nu h_{11/2}$ orbit in the doubly magic ^{132}Sn, i.e., when this orbit is completely filled. All mean-field models using Skyrme and Gogny forces or relativistic NL3 and NL-Z2 forces predict that this high-j orbit is located just below the $N = 82$ gap, the $\nu d_{3/2}$ orbit being more bound by about 1 MeV (see Figure 7 of Ref. [66]), while the ground state of ^{131}Sn has spin $3/2^+$ and its first excited state at 65 keV has spin $11/2^-$. One surmises that the lack of three-body forces is responsible for the discrepancy. Indeed these forces would strongly enhance the binding energy of the filled $\nu h_{11/2}$ orbit.

6.2.6. **A new sub-shell closure at $N = 90$?** An interesting effect of the three-body forces would be the creation of a gap at ^{140}Sn$_{90}$, between the $2f_{7/2}$ and $2p_{3/2}$ shells, as proposed by Sarkar *et al* [67]. Indeed the neutron-neutron monopole terms (and possibly the three-body terms) which intervene here are somehow similar to the ones at $N = 28$. The only modifications are that the nodes of the wave functions differ, and that the monopole term for $A \simeq 48$ has to be downscaled to account for the reduction of the interaction energy as the nucleus grows in size at $A \simeq 140$. When using Equation 8, the suitable downscaled monopole terms, and the known $2f_{7/2} - 2p_{3/2}$ spacing of 0.85 MeV in ^{133}Sn [68, 69] it is found that the $N = 90$ gap is expected to grow by about 2.2

MeV while filling the $2f_{7/2}$ orbit. This leads to a subshell gap of about 3.1 MeV at ^{140}Sn. If established, this subshell gap would bring an additional credit to the mechanism of shell gap creation by three-body forces in another region of the chart of nuclides. In addition, this subshell could bring a local waiting point around ^{140}Sn in the r-process nucleosynthesis.

In summary, the three-body forces are needed to create the neutron SO gaps. While these gaps are not obtained when using microscopic effective interaction (see for instance the discussion recently done by Smirnova *et al* [70]), the phenomenologically adjusted values of the TBME or the explicit implementation of the three-body forces in SM approaches generate the expected neutron SO gaps.

6.3. Could we disentangle tensor and spin-orbit forces in the $N = 28$ region ?

6.3.1. **Introduction** The study of the nuclear structure around $N = 28$ has revealed, using the shell model approach, that the tensor and two-body spin orbit interactions are both at play to reduce the proton and neutron gaps far from stability. As proton orbits are degenerate at $N = 28$, these two components could not be disentangled. To separate these components, we propose in this Section to study the evolution of p SO splitting between $^{36}_{16}$S and $^{34}_{14}$Si (a bubble nucleus). We find a sizable reduction of the SO splitting there, which is ascribed to the spin-orbit interaction (and not to tensor or central forces). This assumption comes from the fact that between these two nuclei protons are mainly removed from the $2s_{1/2}$ ($\ell = 0$) orbit, which does not exhibit a specific orientation between the orbital momentum and the intrinsic spin value.

In a second part we propose to use the bubble nucleus $^{34}_{14}$Si to test the density and the isospin-dependent parts of the spin-orbit interaction in mean-field approaches which have never been tested so far. These properties of the spin-orbit interaction are of minor importance in the valley of stability but are crucial at the neutron drip-line and in superheavy nuclei.

6.3.2. **Studying the two-body spin-orbit interaction in the SM approach** As mentioned in Section 3.1, the proton $s_{1/2}$ and $d_{3/2}$ orbits are degenerate at $N = 28$. The reduction of the p SO splitting at $N = 28$, between ^{49}Ca and ^{47}Ar, is due to the combined effects of proton-neutron interactions involving several monopole terms having potentially tensor *and* spin-orbit components. Applying Equation 5 to the p orbits, the SO splitting is:

$$\delta SO(p) = 1.33(V^{pn}_{1d_{3/2}2p_{1/2}} - V^{pn}_{1d_{3/2}2p_{3/2}}) + 0.66(V^{pn}_{2s_{1/2}2p_{1/2}} - V^{pn}_{2s_{1/2}2p_{3/2}}) \quad (10)$$

The two contributions of this Equation can be estimated from the study of the evolution of the p splitting in $N = 21$ nuclei. As the $s_{1/2}$ and $d_{3/2}$ proton orbits are separated by about 2.5 MeV (see ^{35}P in Figure 5), one can therefore assume that these proton orbits are filled *sequentially* in the $N \simeq 20$ isotones. The pairing is providing a small dilution of occupancies among the two orbits as shown in Ref. [42] and Figure 7. Between $^{41}_{20}$Ca$_{21}$

and $^{37}_{16}S_{21}$, four protons are removed. The evolution of the $[\nu 2p_{3/2} - \nu 2p_{1/2}]$ SO splitting writes:

$$\delta SO(p) \simeq 4(V^{pn}_{1d_{3/2}2p_{1/2}} - V^{pn}_{1d_{3/2}2p_{3/2}}) \quad (11)$$

By looking first at the evolution of the neutron $[2p_{3/2}-2p_{1/2}]$ SO splitting between $^{41}Ca_{21}$ and $^{37}S_{21}$ in Figure 11, one investigates the role of proton-neutron interactions involving the $1d_{3/2}$ protons. It is seen that the p SO splitting amounts to 2 MeV in the two nuclei. It follows that the SO splitting does not change between ^{41}Ca and ^{37}S while 4 protons are removed from the $d_{3/2}$ shell, leading to $\delta SO(p) \simeq 0$ and $V^{pn}_{1d_{3/2}2p_{1/2}} \simeq V^{pn}_{1d_{3/2}2p_{3/2}}$. We note that taking the full observed p strength, the conclusion does not change. Indeed the SO splitting amounts to about 1.7 MeV in the two nuclei [59, 71]. We conclude that the spin-dependent part of the $1d-2p$ proton-neutron interaction is small. This is possibly due to the fact that the monopole terms $V^{pn}_{1d_{3/2}2p_{1/2}}$ and $V^{pn}_{1d_{3/2}2p_{3/2}}$ are weak in absolute value, as both their numbers of nodes and orbital momenta differ by one unit.

From these observations, it was inferred also in Ref. [56] that the change of p SO splitting ($\delta SO(p)$) between ^{49}Ca to ^{47}Ar was ascribed to a modest depletion of the $s_{1/2}$ orbit by about 0.66 protons (see also Section 5):

$$\delta SO(p) \simeq 0.66(V^{pn}_{2s_{1/2}2p_{1/2}} - V^{pn}_{2s_{1/2}2p_{3/2}}) \quad (12)$$

Thus at $N \simeq 28$ the effect of the two-body SO interaction is weak. The $N = 21$ region is then more propicious to study this interaction as more protons are depleted in the $2s_{1/2}$ orbit between $^{37}S_{21}$ and $^{35}Si_{21}$.

As for $^{35}Si_{21}$, energies and spectroscopic factors of its first $7/2^-$, $3/2^-$, $1/2^-$ and $5/2^-$ states were determined recently using the (d,p) transfer reaction in inverse kinematics at GANIL. They are compared to those of the isotone $^{37}S_{21}$ [72] in Figure 11. The observed p SO splitting changes by about 900 keV between ^{37}S and ^{35}Si while protons are removed from the $2s_{1/2}$ orbit. This variation is observed in the *major* fragment of the single-particle strength, which contains correlations beyond the monopole terms. In order to unfold these correlations and to derive the change in monopole, the SM approach is used. While adjusting the monopole terms used in the SM calculations in order to reproduce the correlated experimental data [73], a decrease of the p SO splitting from 2 MeV to 1.73 MeV is found for ^{37}S and an increase from 1.1 MeV to 1.35 MeV is found for ^{35}Si. It follows that the change in $[p_{3/2} - p_{1/2}]$ spin-orbit splitting ($\delta SO(p)$) amounts to about 25%, namely $(1.73 - 1.35) = 0.38$ MeV compared to the mean value $(1.73 + 1.35)/2 = 1.54$ MeV. This change is mainly ascribed to a change in the proton $2s_{1/2}$ occupancy which is calculated to be $\Delta(2s_{1/2})$=1.47 :

$$\delta SO(p) \simeq 1.47(V^{pn}_{2s_{1/2}2p_{1/2}} - V^{pn}_{2s_{1/2}2p_{3/2}}) = \ 380 \ keV \quad (13)$$

Note that by using the monopole terms ($V^{pn}_{2s_{1/2}2p_{1/2}}$ and $V^{pn}_{2s_{1/2}2p_{3/2}}$) derived in Section 5 and Figure 9, one finds using Equation 13 a consistent change in the p SO splitting of 1.47(85+170)= 370 keV between ^{37}S and ^{35}Si*. The present change in SO splitting

* In practice the monopole terms should be slightly renormalized according to the $A^{1/3}$ scaling rule between $A \simeq 48$ and $A \simeq 36$ region

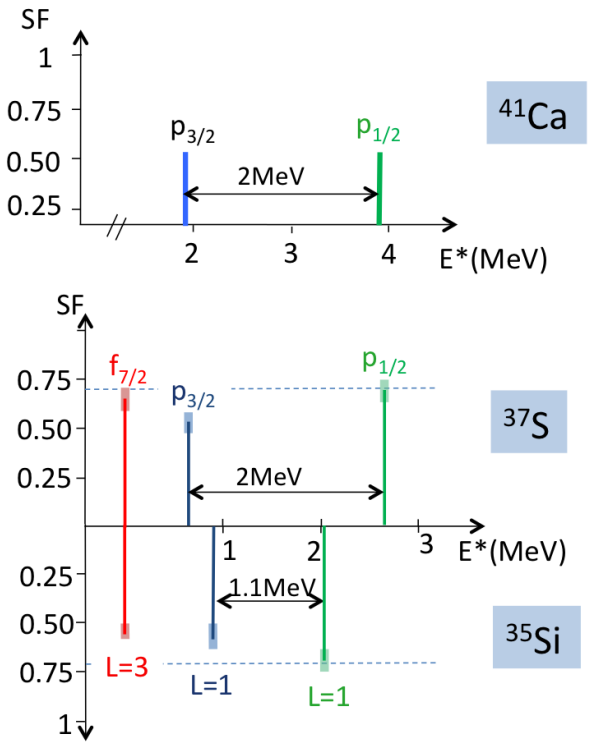

Figure 11. Distribution of the major fragments of the single-particle strengths in the $N = 21$ isotones. Spectroscopic factors are represented in the y axis (adapted from Ref. [72]).

is *exclusively* due to the two-body spin-orbit force, as monopole terms involving an $\ell = 0$ component, as it does here with the $s_{1/2}$ orbit, does not contain any tensor component [30]. The only worry for this extraction of two-body term comes from the fact that the energy and wave function of $1/2^-$ state in ^{35}S, which is bound by about 0.5 MeV, may be influenced by the proximity of the continuum.

Having an orbital momentum ℓ=0, the $2s_{1/2}$ orbit is located in the center of the nucleus. With a weak $2s_{1/2}$ occupancy, ^{34}Si is expected to have a depleted proton central density [74] in the SM as well as in the MF approaches. This depletion is also seen in the density profile calculated using the RMF/DDME2 interaction [75] in the left part of Figure 12. On the other hand, the proton densities of the other $N = 20$ isotones do not display any central depletion (see the middle and the right part of Figure 12). With this peculiarity of density depletion *and* isospin difference in central density (proton and neutron density profiles differ significantly), the ^{34}Si nucleus is a good candidate to study the SO interaction in mean-field approaches, as described below.

6.3.3. **The spin-orbit interaction in the mean-field approaches** Interesting is to note that all theoretical approaches do not agree on the reason for the $N = 28$ shell disappearance. Li *et al* [18] say that the '*RMF model automatically reproduces the*

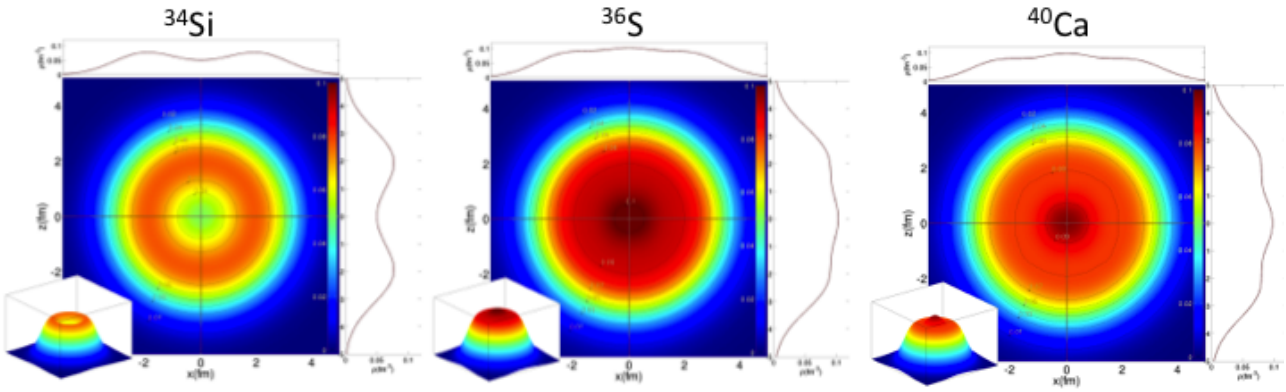

Figure 12. Proton density profiles obtained with the RMF/DDME2 calculation in the $N = 20$ isotones. From the left-hand picture, it is seen that the ^{34}Si nucleus displays a central depletion. By courtesy of J.P. Ebran.

$N = 28$ *spherical shell gap because it naturally includes the spin-orbit interaction and the correct isospin dependence of this term'*. Therefore in the RMF approach '*there is no need for a tensor interaction to reproduce the quenching of the spherical* $N = 28$ *gap in the neutron-rich nuclei'*.. The bubble nucleus ^{34}Si will be used to ascertain these statements.

Relativistic Mean Field (RMF) models introduced description of the nuclear spin-orbit interaction [76] in terms of mesonic degrees of freedom, treating the nucleons as Dirac particles. Using a non-relativistic reduction of the Dirac equation, the spin-orbit term writes:

$$V_\tau^{ls}(r) = -[W_1 \partial_r \rho_\tau(r) + W_2 \partial_r \rho_{\tau\neq\tau'}(r)] \overrightarrow{\ell} \cdot \overrightarrow{s} \tag{14}$$

in which W_1 and W_2 depend on the σ, ω, ρ meson coupling constants, and τ represents a proton or a neutron. Note that the W_1 and W_2 parameters have also density dependence in the RMF calculations that we neglect here. Thus beyond the $\ell \cdot s$ term, the SO interaction contains a *density* dependence through $\partial_r \rho(r)$ and an *isospin* dependence through the W_1/W_2 ratio. Both relativistic and non-relativistic mean-field (MF) approaches agree on a significant density dependence of the spin-orbit interaction. However, while there is moderate isospin dependence of the SO interaction in the RMF approach ($W_1/W_2 \simeq 1$), non-relativistic Hartree-Fock approaches have a large isospin dependence (W_1/W_2=2) provided by the exchange term [77] of the nuclear interaction. Beyond the fundamental importance to describe the spin orbit interaction, the density and isospin dependences of the spin-orbit interaction have important consequences to model nuclei close to the drip-line [78], to predict the isotopic shifts in the Pb region [79] and to describe superheavy nuclei which display a central-density depletion [80].

Having a significant proton-density depletion and a proton-neutron density asymmetry (there is no neutron central depletion), the ^{34}Si nucleus is a good candidate to study both the density and isospin dependence of the spin-orbit interaction as proposed

in Ref. [72]. Indeed RMF models give a large change in SO splitting by about 80% between ^{37}S and ^{35}Si while MF models find a more modest change of about 30% for $\Delta(2s_{1/2})$ =1.5 [72].

The presently observed decrease of the SO splitting between ^{37}S and ^{35}Si by about 25% indicates that there is a density dependence of the SO interaction, otherwise no change in SO splitting would have been found. This modest change is in better agreement with theoretical models having a *large* isospin dependence, such as most of the MF models. Though extremely preliminary, this discovery would suggest that the treatment of the isospin dependence of the SO interaction in the RMF approach is not appropriate. If true this would have important consequences to model nuclei which are sensitive to the isospin dependence of the SO interaction. We give here two examples.

In some superheavy nuclei, large proton and neutron central-density depletion may be present. They originate from the coulomb repulsion between protons and from the filling of high-j neutron orbits which are located at the nuclear surface only [80]. Assuming no isospin dependence of the SO interaction as in the RMF approach, the proton and neutron central-density depletions *mutually* reduce the proton SO splitting for (ℓ =1, 2, and 3) orbits which are probing the interior of the nucleus [80]. In this case, the $Z = 114$ gap, formed between the proton $f_{5/2}$ and $f_{7/2}$ would be significantly reduced to the benefit of a large shell gap at $Z = 120, N = 172$. Conversely, a rather large isospin dependence of the SO interaction would not lead to strong shell gaps [81] but rather to sub-shells the rigidity of which is further eroded by correlations. The second example deals upon nuclei close to the neutron drip-line. As they are expected to have a smoothened neutron density at their surface, the spin-orbit of high-j orbits is expected to be weakened.

In the RMF approach the SO interaction is weaker by about up to 65% as compared to MF approaches when reaching the drip -line [78]. This change between RMF and MF models seems to be due to the different treatment of the isospin dependence of the SO interaction [78]. This change in SO interaction could have important consequences to model the evolution of the $N = 28$ shell closure far from stability as well as other SO magic numbers along which the r-process nucleosynthesis occurs [82]. We note here that other competing effects come into play to modify shell structure when approaching the drip-line, as mentioned in the following Sections.

6.4. Would other SO magic numbers 14, 50, 82 be disappearing far from stability as $N = 28$ does and if not why ?

6.4.1. **Introduction** In this Section we look whether the SO magic gaps $14, 50, 82$ are progressively vanishing when moving far from stability in the same manner as $N = 28$ does toward ^{42}Si. We start with the analogy of the evolution of the $N = 14$ shell gaps between ^{22}O and ^{20}C and pursue with the evolution of the SO magic number in the ^{132}Sn nucleus at $N = 82$. We show that, surprisingly, while the same forces are involved in all regions, the $N = 82$ gap remains very large contrary to the $N = 14$ and $N = 28$ ones.

The ^{78}Ni nucleus, which lies in between the ^{42}Si and ^{132}Sn nuclei, is briefly discussed as well.

6.4.2. **Disappearence of the $N = 14$ and $N = 28$ gaps far from stability** The $N = 28$ gap vanishes progressively by the removal of 6 protons from the doubly magic ^{48}Ca to the deformed ^{42}Si nucleus. As far as tensor forces are concerned, their action cancels in a spin saturated valence space, i.e., when orbits with aligned and anti-aligned spin orientations with respect to a given angular momentum are filled. In the present valence space for instance, the filling of the proton $f_{7/2}$ and $f_{5/2}$ annihilates the tensor effects on the filled $d_{5/2}$ and $d_{3/2}$ orbits. As the ^{42}Si nucleus is a spin unsaturated system in protons and neutrons, tensor effects are maximized, leading to reductions of both the proton $d_{3/2} - d_{5/2}$ and neutron $f_{7/2} - f_{5/2}$ splittings. Similar spin unsaturated nuclei exist in nature, such as (i) ^{20}C ($\pi p_\uparrow$ and $\nu d_\uparrow$ filled but not $\pi p_\downarrow$ and $\nu d_\downarrow$), (ii) ^{78}Ni ($\pi f_\uparrow$ and $\nu g_\uparrow$ filled but not $\pi f_\downarrow$ and $\nu g_\downarrow$) and (ii) ^{132}Sn ($\pi g_\uparrow$ and $\nu h_\uparrow$ filled but not $\pi g_\downarrow$ and $\nu h_\downarrow$). These examples are illustrated in Figure 13. We would expect that the behavior of all these four mirror valence nuclei is similar, but it is not the case.

Starting with the first example, $N = 14$, it was found in Ref. [83] that the energy of the first 2^+ state drops by a factor of two between ^{22}O (3.2 MeV [84]) and ^{20}C (1.588 MeV). Then the reduction of the $N = 14$ gap, formed between the neutron $d_{5/2}$ and $s_{1/2}$ orbits, could be ascribed to the two monopole interactions involved when removing 2 protons from the $p_{1/2}$ orbit between ^{22}O and ^{20}C, i.e.:

$$\delta G^{pn}(14) \simeq 2(V^{pn}_{1p_{1/2}2s_{1/2}} - V^{pn}_{1p_{1/2}1d_{5/2}}) \tag{15}$$

We can estimate the reduction of the $N = 14$ gap by looking at similar forces in the valley of stability. The ordering of the $d_{5/2}$ and $s_{1/2}$ is exchanged between ^{17}O (g.s. $5/2^+$, $1/2^+$ at 870 keV) and ^{15}C (g.s. $1/2^+$, $5/2^+$ at 740 keV). Such a swapping of about 1.6 MeV between the two neutron orbits means that $|V^{pn}_{1p_{1/2}1d_{5/2}}| >> |V^{pn}_{1p_{1/2}2s_{1/2}}|$. The large value of the $|V^{pn}_{1p_{1/2}1d_{5/2}}|$ monopole can be ascribed to the attractive part of the tensor term. Assuming that the two monopoles are of similar intensity between $A = 16$ and $A = 22$, the $N = 14$ gap is expected to be reduced by 1.6 MeV between ^{22}O and ^{20}C, starting from a value of about 4 MeV in ^{22}O (see Figure 10). This large reduction of the $N = 14$ spherical gap, by the removal of only two protons, can easily account for the decrease in 2^+ energy in ^{20}C.

For the $N = 28$ shell gap, the removal of 6 protons is required to change drastically the nuclear structure. The effect of residual forces per nucleon is less important than in the lighter nuclei. It is also noticeable that the size of the $N = 28$ gap (4.8 MeV) is about 1 MeV larger than that of $N = 14$. These two effects, weaker monopole terms and increasingly larger SO splitting, could explain why the vanishing of the shell gap occurs further from stability at $N = 28$.

6.4.3. **Persistence of the $N = 82$ gap in ^{132}Sn** On the other hand, ^{132}Sn has all the properties of a doubly-magic nucleus with a high 2^+ energy of 4.04 MeV [85], due

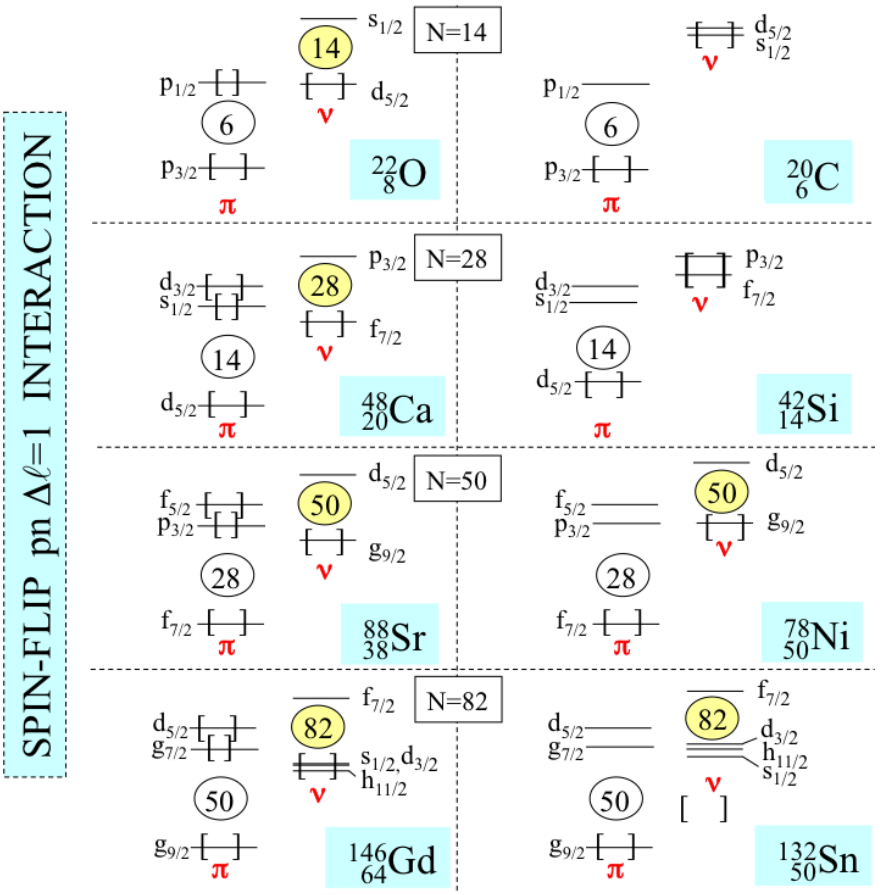

Figure 13. Schematic evolution of the SO shell gaps at N =14, 28, 50 and 82 as a function of the filling of the proton $\ell \downarrow$ orbits, with ℓ =1, 2, 3 and 4, respectively. While the $N = 14$ and $N = 28$ magic gaps vanish in nuclei far from the stability valley (right column), the $N = 50$ gap slightly decreases and the $N = 82$ one remains very robust.

to a large shell gap [3]. Large spectroscopic factors are found in the ^{132}Sn (d,p) ^{133}Sn reaction [69, 86], which is a further confirmation that ^{132}Sn is a closed-shell nucleus. Note that the $N = 82$ gap is not strictly formed between the neutron $h_{11/2}$ and $f_{7/2}$ orbits, as the $h_{11/2}$ orbit lies below the $d_{3/2}$ one for $Z = 50$ [87]. This arises from the fact that the $h_{11/2} - h_{9/2}$ SO splitting is larger than the other SO splittings $g_{9/2} - g_{7/2}$, $f_{7/2} - f_{5/2}$ and $d_{5/2} - d_{3/2}$ in the $N = 50$, $N = 28$ and $N = 14$ regions respectively. This increasingly large splitting with ℓ value is due to the $\overrightarrow{\ell} \cdot \overrightarrow{s}$ term of Equation 14.

6.4.4. **The $N = 50$ shell gap in ^{78}Ni** In the $N = 50$ case, the rigidity of the ^{78}Ni nucleus with respect to quadrupole excitations is not known so far. Based on the study of spectroscopic information between $Z = 30$ and $Z = 38$, the evolution of the $N = 50$ shell gap has been studied in Ref. [64]. A rather modest reduction of about 0.55 MeV was proposed between $Z = 38$ and $Z = 28$. Nevertheless, as this reduction is combined

with that of the $Z = 28$ gap [65], it is not absolutely sure that ^{78}Ni would remain spherical in its ground state.

6.4.5. **Conclusions** Though similar tensor and spin-orbit forces are at play for $N = 14$, 28, 50 and 82, the corresponding shell closures do not have the same behavior when going far from stability. Quadrupole correlations dominate in $N = 14$ and $N = 28$ over the spherical shell gaps, while the $N = 82$ gap remains remarkably rigid in ^{132}Sn. This feature likely comes from two effects : (i) the SO shell gaps become larger for higher ℓ orbits and (ii) the monopole terms involved to reduce the shell gap are weakened in heavy nuclei because of the larger sizes of the orbits. In the next Section we explore the forces which come into play even further from stability.

6.5. Which forces come into play in nuclei located below ^{42}Si, ^{78}Ni and ^{132}Sn?

6.5.1. **Introduction** Advances in radioactive beam productions offer the possibility to produce and study nuclei at the limit of particle stability. There, new forces are involved and the interaction with continuum states should progressively play a decisive role. We start this Section by a qualitative analysis of the nuclear forces involved at $N = 28$ below ^{42}Si. We propose that this gap is further reduced, and illustrate our purpose by looking at recent experimental studies which evidence the inversion between the $f_{7/2}$ and $p_{3/2}$ orbits. We generalize this mechanism to other shell gaps, $N = 50$ and $N = 82$, and propose astrophysical consequences for the r-process nucleosynthesis below ^{132}Sn.

6.5.2. **The $N = 28$ shell gap below ^{42}Si** It was shown in Refs. [88, 34] that the neutron drip line extends further $N = 28$ in the Si and Al isotopic chains, i.e., at least up to ^{44}Si$_{30}$ and ^{43}Al$_{30}$, respectively. If the $N = 28$ shell gap was large, a sudden drop in S_{2n} would be found there and the drip-line would lie at $N = 28$ and not beyond. To give an example, the neutron drip line is exactly located at a magic shell in the O chain, where ^{24}O is bound by about 3.6 MeV and ^{25}O is unbound by about 770 keV [89]. So in this case, ^{24}O is a doubly-magic nucleus [90, 91, 92] and the spherical shell gap is large enough to hamper the onset of quadrupole correlations. By contrast the fact that the drip line extends further from stability at $N = 28$ is an indication for the presence of deformed nuclei which gain in binding energy due to correlations. This also hints for a further reduction of the $N = 28$ shell gap. This hypothesis is hard to prove in a direct way as it would require to determine the size of the spherical shell gap there, which is out of reach so far, and which would not be an observable when nuclei are deformed. Therefore we shall use qualitative arguments as well as an example taken from another region of the chart of nuclides where similar forces are present to predict the behavior of the $N = 28$ shell gap further from stability. With this in mind, we will propose some extrapolations to other regions of the chart of nuclides.

Below ^{42}Si the change of the $N = 28$ shell gap between the $1f_{7/2}$ and $2p_{3/2}$ orbits

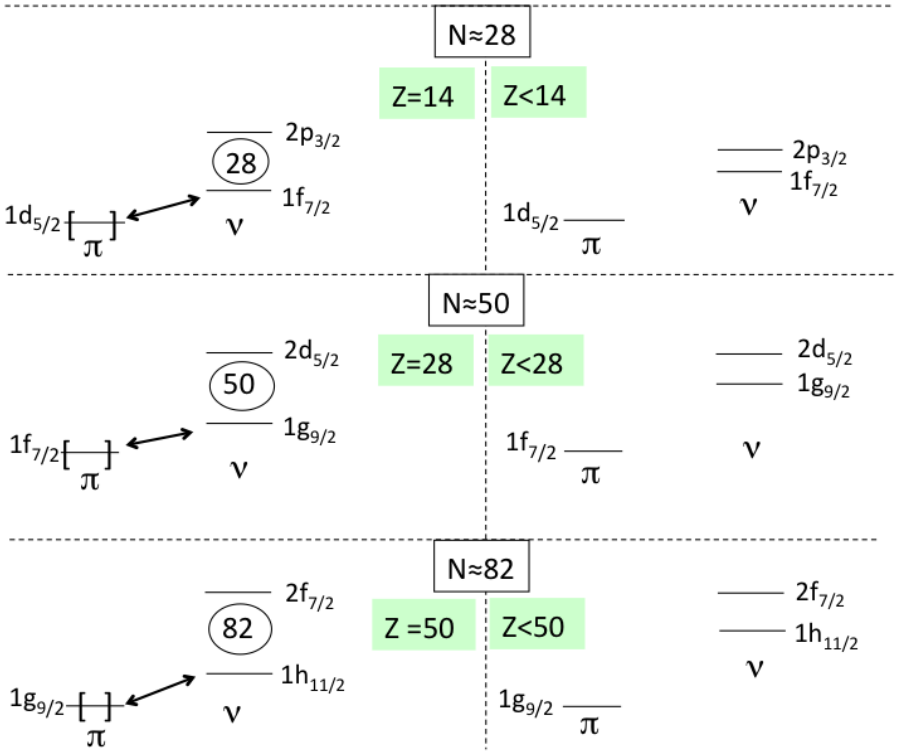

Figure 14. Schematic evolution of the SO shell gaps at 28, 50 and 82, as a function of the filling of the proton $\ell\uparrow$ orbits, with ℓ =2, 3 and 4, respectively. The attractive pn interaction $1d_{5/2}-1f_{7/2}$ is larger than the $1d_{5/2}-2p_{3/2}$ one. Therefore the $N = 28$ gap is larger when the $d_{5/2}$ orbit is completely filled (left part). Conversely, when emptying the $\pi d_{5/2}$ orbit (i.e., going very far from stability) the $N = 28$ gap is expected to vanish (right part). The same mechanism is foreseen for the N =50 (82) gap when the $\pi f_{7/2}$ ($g_{9/2}$) orbit is empty.

is driven by the difference between the $V^{pn}_{1d_{5/2}2p_{3/2}}$ and $V^{pn}_{1d_{5/2}1f_{7/2}}$ monopole terms. On top of this monopole-driven effect, correlations play an important role in these nuclei. For these two monopole terms, the proton and neutron spin orientations are aligned with the orbital momentum, and their difference in angular momentum is one unit of $\hbar$ (then the main part of the proton-neutron interaction comes from the central term of the nuclear force). On the other hand, the numbers of nodes in their wave functions are different. The fact that the $1f_{7/2}$ and $1d_{5/2}$ wave functions have the same number of nodes leads to a larger radial overlap of the wave functions, and a larger monopole term $V^{pn}_{1d_{5/2}1f_{7/2}}$ as compared to $V^{pn}_{1d_{5/2}2p_{3/2}}$. Consequently when the $1d_{5/2}$ orbit is completely filled, the $1f_{7/2}$ orbit has a larger binding energy than that of the $2p_{3/2}$ one. Conversely, when removing the six protons from the $1d_{5/2}$ orbit, the neutron $N = 28$ gap further shrinks. Note that the calculations of Ref. [32] predict a decrease by 1.6 MeV down to $^{36}O_{28}$. Of course this nuclei lies beyond the drip-line, but this gives the monopole trend for the evolution of the $N = 28$ gap below ^{42}Si (see Figure 14).

In addition to this monopole effect, the nuclear-potential well will become more

diffuse when moving towards the drip-line. It was proposed by Dobaczweski *et al* [93] that this would bring the low ℓ orbits more bound as compared to the high ℓ ones, which could be viewed schematically as a reduced ℓ^2 term in the Nilsson potential. Then, an inversion of the two negative-parity orbits (f and p) could also happen, as suggested by several experimental works described below.

While the $\nu 1f_{7/2}$ orbit lies below the $\nu 2p_{3/2}$ orbit in most of the nuclei in the chart of nuclides (giving rise to the $N = 28$ shell gap), their ordering is reversed as soon as the $\pi d_{5/2}$ shell starts to empty, i.e., for $Z < 14$. The feature is well documented in the $N = 15$ and $N = 17$ isotones, not far from the stability valley. Indeed, the first negative-parity state of $^{29,31}_{14}\mathrm{Si}_{15,17}$ has $I^\pi = 7/2^-$ while the $3/2^-$ state is located above. On the other hand, the situation is reversed in $_{12}$Mg and $_{10}$Ne isotopes, as described now. In the $^{25}\mathrm{Ne}_{15}$ nucleus [94], the $2p_{3/2}$ orbit lies about 1 MeV *below* the $1f_{7/2}$ orbit. This was determined by using the ^{24}Ne(d,p)^{25}Ne transfer reaction in inverse kinematics at the GANIL facility. Similar results were recently obtained at GANIL in $^{27}\mathrm{Ne}_{17}$, its first excited state at 765 keV having $I^\pi = 3/2^-$ [95], the $7/2^-$ state being about 1 MeV above. Note that the assignment of the $3/2^-$ state was first proposed in Refs. [96, 97]. In the neighboring isotone ^{29}Mg, the second excited state at 1095 keV was observed from the study of the β decay of ^{29}Na. It could not be explained in the framework of shell-model calculations using the *sd* space, and consequently it was assigned as a $I^\pi = 3/2^-$ intruder state [98]. To our knowledge, two other experimental works are suggesting this inversion between the $1f$ and $2p$ orbits. By using Coulomb break-up technique at RIKEN, Nakamura *et al* [99] found that the ground-state wave function of ^{31}Ne was dominated by an $\ell = 1$ component. Minomo *et al* [100] propose a contribution of a $p_{3/2}$ neutron using antisymmetrized molecular dynamics calculations. Moreover Wimmer *et al* argued that excitations to the $2p_{3/2}$ (rather than the $1f_{7/2}$) are required to account for the configuration of the $0^+_{1,2}$ states in ^{32}Mg determined through two-neutron transfer reaction at CERN/ISOLDE [101]. In these examples, in which the proton $1d_{5/2}$ orbit is not yet fully filled, the $N = 28$ gap does not exist and the $\nu 2p_{3/2}$ orbit even lies below the $\nu 1f_{7/2}$ orbits. Conversely, this gives a further indication that the proton $1d_{5/2}$ has to be filled to bind the $\nu 1f_{7/2}$ orbit enough to create a $N = 28$ gap which is present in heavier nuclei. Note that, from a theoretical point of view, this inversion was also proposed by Utsuno *et al* in 1999 [102].

6.5.3. **Extrapolations to other shells $N = 50$ and $N = 82$** We can reasonably assume that the present mechanism for the reduction of the $N = 28$ gap is robust, as it comes from the radial part of the wave functions and from the effect of a more diffused potential well at the drip-line. As far as the first effect is concerned, it is also observed from the properties of the bare proton-neutron forces [103]. We therefore also expect the reduction of the $N = 50$ gap below ^{78}Ni and the reduction of the $N = 82$ gap below ^{132}Sn, as protons are removed from the $1f_{7/2}$ and $1g_{9/2}$ orbits, respectively (see Figure 14). While the $N = 82$ gap is still present in the ^{132}Sn nucleus, it will progressively be reduced further from stability as ten protons are removed from the

$1g_{9/2}$ orbit to reach ^{122}Zr. The onset of quadrupole correlations across the $N = 82$ shell gap would occur if the neutron gap is reduced enough. This would bring a smoothening in the S_{2n} trend, as observed in Figure 2 for the $N = 28$ isotones around ^{44}S. This has potentially important consequences on the location of the $(n, \gamma) - (\gamma, n)$ equilibrium in the rapid neutron-capture process (r-process). This equilibrium occurs when neutron captures compete with photo-disintegrations. At this point, further neutron captures cannot occur as nuclei are immediately destroyed. Therefore the explosive process is stalled for a moment at such waiting-point until β-decay occurs. When the drop in S_{2n} value is abrupt (for a large shell gap), the waiting-point nuclei are found *at* the closed shell. Then these nuclei are the main genitors of stable r-elements when decaying back to stability. When the shell gap is reduced, the location of r-progenitors is more extended and shifted to lower masses in a given Z chain, changing the fit of the r-process abundance curve accordingly (see for instance Ref. [82]).

To summarize this Section, we propose that both from the nuclear two-body forces and from the mean-field point of views a further reduction of the $N = 28$ shell gap will be occurring below ^{42}Si. By analogy, a reduction of the $N = 50$ and $N = 82$ shell gaps is anticipated, with possible important consequences for the r-process nucleosynthesis in the later case.

6.6. Are proton-neutron forces significantly modified when approaching the drip line ?

6.6.1. **Introduction** In the previous Sections we assumed that the two-body proton-neutron forces (or the monopole terms) remain of similar intensity when reaching the drip line. The SM description does not allow a self-consistent change of the monopole terms as a function of binding energy. However the assumption of fixed monopole terms in a wide valence space is at best crude and probably wrong. Indeed at the neutron drip-line, valence protons are very deeply bound and their wave functions are well confined. On the other hand, neutrons, which are close to be unbound, have more dilute wave functions and interactions with continuum states occur [104]. It follows that the radial part of the wave functions of the valence proton and neutron have weaker overlap, leading to a reduced effective interaction. One could question by how much this interaction is reduced ?

The $_9$F isotopic chain is a target choice to study changes in proton-neutron forces when approaching the drip line. Indeed the drip-line occurs at $N = 16$ in the $_8$O chain, i.e., at ^{24}O, while the ^{31}F$_{22}$ nucleus is still bound. Thus the addition of a *single* proton allows to bind up to 6 neutrons more. It follows that, though occurring between nuclei showing large asymmetry in neutron and proton binding energy, the corresponding proton-neutron forces should be large enough to bind ^{31}F$_{22}$♯. Up to ^{29}F$_{20}$, the same proton-neutron $d_{5/2} - d_{3/2}$ is expected to intervene. This strong monopole force is well known to produce significant changes closer to stability in the shell evolution of the

♯ Beyond proton-neutron interactions, we remind here the important role of neutron-neutron forces as well.

$N = 16$ and $N = 20$ gaps. How is this force modified far from stability ? The recent determinations of the binding energies of the (unbound) $^{28}F_{19}$ [105] and the bound $^{29}F_{20}$ [106] offer the possibility to start answering these questions. However error bars on binding energies are still a bit too large at present to draw firm conclusions.

In this Section we propose to study the spectroscopy of the $^{26}_{9}F_{17}$ to study the proton-neutron $d_{5/2} - d_{3/2}$ interaction when approaching the drip line. We first explain the motivation of studying this nucleus and subsequently use the new spectroscopic information required to study the proton-neutron force.

6.6.2. **Experimental study of $^{26}_{9}$F** The $^{26}_{9}F_{17}$ nucleus is a suitable choice for studying the proton-neutron $d_{5/2} - d_{3/2}$ interaction for at least three arguments: (i) it is bound by only 0.80(12) MeV, (ii) as the first excited state in ^{24}O lies at 4.47 MeV [91], ^{26}F can be viewed as a closed ^{24}O core plus a *deeply bound* proton in the $d_{5/2}$ orbit ($S_p(^{25}\mathrm{F}) \simeq$ -15 MeV) and an *unbound* neutron in the $d_{3/2}$ orbit ($S_n(^{25}\mathrm{O}) \simeq +0.77$ MeV [89]), (iii) the $\pi d_{5/2}$ and $\nu d_{3/2}$ orbits are rather well separated from other orbits which limit correlations of pairing and quadrupole origin. Binding energies BE(^{26}F)$_J$ of the *full* multiplet of $J = 1 - 4^+$ states arising from the $\pi d_{5/2} \otimes \nu d_{3/2}$ coupling in $^{26}_{9}F_{17}$ are needed to determine the role of the coupling to the continuum on the mean $\pi d_{5/2} \nu d_{3/2}$ interaction energy (int), defined in Equation (16), as well as on the residual interaction which lifts the degeneracy between the components of the multiplet $int(J)$ defined in Equation (17). The mean interaction energy (int) writes:

$$int = \sum \frac{(2J+1) \times int(J)}{(2J+1)} \tag{16}$$

In this Equation $int(J)$ term expresses the difference between the experimental binding energy of a state J in ^{26}F (BE(^{26}F)$_J$) and that of the ^{24}O+1p+1n system, $BE(^{26}F_{free})$, in which the valence proton and neutron do not interact. It writes:

$$int(J) = BE(^{26}F)_J - BE(^{26}F_{free}), \tag{17}$$

where

$$BE(^{26}F_{free}) = BE(^{24}O)_{0^+} + BE(\pi d_{5/2}) + BE(\nu d_{3/2}) \tag{18}$$

Assuming that

$$BE(\pi d_{5/2}) = BE(^{25}F)_{5/2^+} - BE(^{24}O)_{0^+} \tag{19}$$

and

$$BE(\nu d_{3/2}) = BE(^{25}O)_{3/2^+} - BE(^{24}O)_{0^+} \tag{20}$$

we obtain:

$$BE(^{26}F_{free}) = BE(^{25}F)_{5/2^+} + BE(^{25}O)_{3/2^+} - BE(^{24}O)_{0^+} \tag{21}$$

Following the particle-particle coupling rule, the values of $int(J)$ should display a parabola as a function of J in which $|int(1)|$ and $|int(4)|$ are the largest, as proton and neutron maximize their wave-function overlap for these two values of total angular

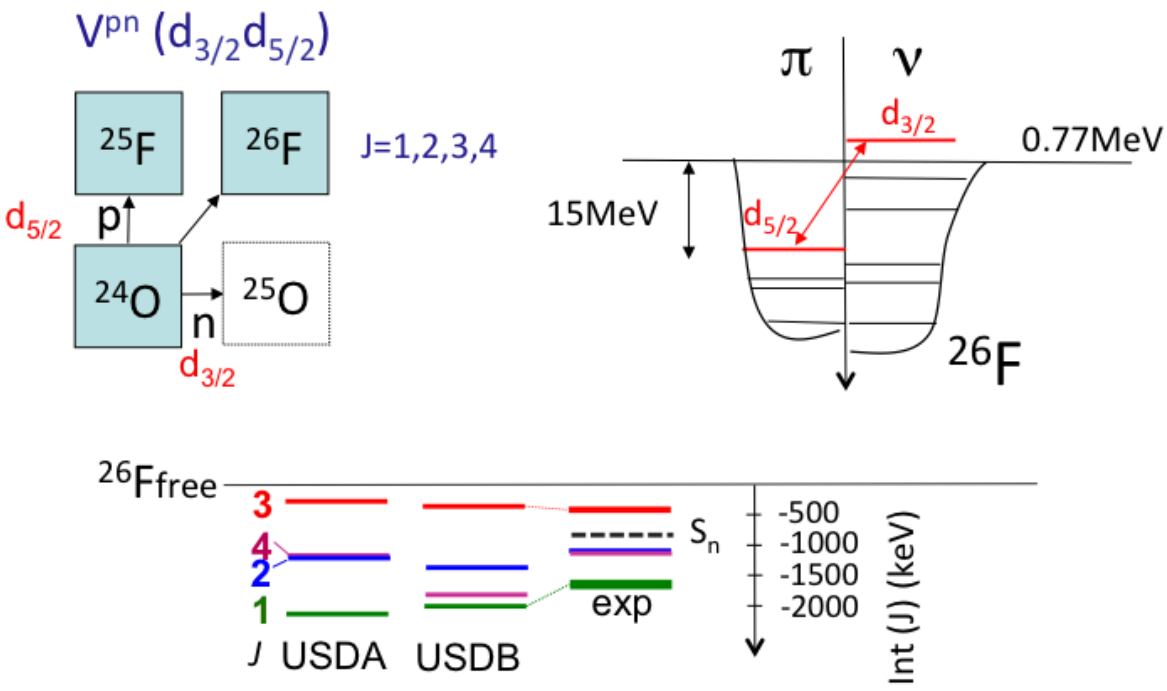

Figure 15. Schematic view of the low-energy configurations in ^{26}F, which could be approximated as a core of ^{24}O on top of which a deeply bound proton $d_{5/2}$ and an unbound neutron $d_{3/2}$ are added. This could bring, after having treated the role of correlations, information on the proton-neutron $d_{5/2} - d_{3/2}$ interaction close to the drip-line. In the bottom part, values of int(J) extracted from the SM calculations are compared to the presently known experimental values for $J^\pi = 1^+ - 4^+$.

momentum, leading to the largest attractive interactions. The values of $int(J)$ obtained from shell model calculations (see bottom part of Figure 15) indeed form a parabola, the $|int(3)|$ value being the lowest.

The atomic masses of ^{26,25}F and ^{24}O were determined by Jurado *et al* [4]. They were used to determine the binding energies BE values used in the previous Equations. The $BE(^{25}O)_{3/2^+} - BE(^{24}O)_{0^+}$=+0.77 MeV difference is derived from the work of Hoffman *et al* [89]. The spin of the ground state of ^{26}F was determined to be $I^\pi = 1^+$ by Reed *et al* [107] from the fact that $I^\pi = 0, 2^+$ states were populated in its β decay. The first-excited state of ^{26}F has been recently identified at 657(7) keV excitation energy by Stanoiu *et al* [108] at GANIL using in-beam γ-ray detection combined to the double fragmentation method. Moreover, an unbound state lying 270 keV above the neutron emission threshold has been proposed by Franck *et al* following a nucleon-exchange reaction at NSCL [109]. This state is likely to be the $I^\pi = 3^+$ state. Finally a long-lived $J = 4^+$ isomer, $T_{1/2} = 2.50(5)$ms, has been discovered at 642 keV by Lepailleur *et al* at GANIL [110]. It decays by an $M3$ internal transition to the $J = 1^+$ ground state (86%), and by beta-decay to ^{26}Ne or beta-delayed neutron emission to ^{25}Ne. Gathering

the measured binding energies of the $J = 1 - 4^+$ multiplet in $^{26}_{9}$F in Figure 15 †† we find that the components of the multiplet are experimentally more compressed than the SM predictions, whatever the effective interaction, USDA or USDB [111] . This would be due to a weaker residual interaction $\pi d_{5/2}\nu d_{3/2}$ close to the drip line. It would be interesting to compare these findings to calculations taking into account the effect of continuum. Note that the present conclusions rely strongly on atomic mass determination of the $^{26}_{9}$F ground state, as well as the resonance at ∼270 keV we have assigned to be the $I^\pi = 3^+$ state of the multiplet. These two results deserve to be confirmed.

7. General conclusions

The evolution of the $N = 28$ shell closure has been investigated far from stability, showing a reduction of the spherical shell gap. It was found that a progressive onset of deformation occurs after the removal of several protons. Starting from a rigid-spherical $^{48}_{20}$Ca nucleus, $^{46}_{18}$Ar has a vibrational character, $^{44}_{16}$S exhibits a shape coexistence, $^{42}_{14}$Si is likely to be oblate and $^{40}_{12}$Mg is expected to be prolate. Adding the triaxiality in the ^{48}Ar nucleus, a wealth of nuclear structures can be explored in this mass region.

This structural evolution has been probed using various experimental techniques, such as in-beam γ-ray spectroscopy, transfer, Coulomb excitation, g factor measurement; to quote a few. The evolution of the *sd* proton and *fp* neutron orbits was probed, from which important conclusions were derived. Starting with proton orbits, a total disruption of the $Z = 16$ sub-shell, formed between the $s_{1/2}$ and $d_{3/2}$ orbits, occurs from $N = 20$ to $N = 28$. In parallel a reduction of the $Z = 14$ gap (between the $d_{5/2}$ and $s_{1/2}$ orbits) seems to be present as well. This global shrink between proton states favors the development of pairing and quadrupole excitations at $N = 28$ as compared to $N = 20$, where the magicity persists down to $^{34}_{14}$Si. As for neutrons orbits, reductions of the *f* and *p* SO splittings as well as the $N = 28$ shell gap (by about 25%) were proposed between ^{48}Ca and ^{42}Si. This reduction is large enough to trigger the development of quadrupole excitations across the $N = 28$ gap. In all, both the proton and neutron shell gaps are reduced in the spin-unsaturated ^{42}Si nucleus, mutually enhancing the collectivity there.

These studies have in addition shown the many facets of nuclear force that can be explored, such as the central, spin-orbit, tensor and three-body terms. It also triggered the question of proton-neutron forces below ^{42}Si and more generally when approaching the drip-line. These points were addressed in the last part of the manuscript. Conclusions are as follows:

- Due to three-body effects, the $N = 28$ gap grows from $N = 20$ to $N = 28$ by about 2.7 MeV. As similar forces seem to be at play in the other SO shell gaps, an empirical rule was proposed to predict the increase of the $N = 14$, $N = 50$, $N = 82$ shell gaps when the $\ell \uparrow$ orbits (with ℓ =2,3,4) are completely filled. Following this

†† The atomic mass of ^{26}F measured in [4] was shifted to a larger binding energy (downward) to take into account the probable contamination of 40% in isomeric state.

rule, a new $N = 90$ sub-shell gap should be present in ^{140}Sn, leading to interesting consequences for the r-process nucleosynthesis.

- The roles of the central, tensor and spin-orbit components of the nuclear force were examined in the framework of the shell model using various experimental data. The bubble nucleus ^{34}Si has been used to probe the reliability of the density and isospin dependence of the SO interaction in mean-field models. It was derived that the spin-orbit interaction is indeed density dependent, but also seems to have an important isospin dependence that is not present in RMF approaches. This feature should have significant consequences to model the structure of superheavy and neutron-rich nuclei, which exhibit central density depletion and surface diffuseness, respectively.
- Below ^{42}Si, central forces further reduce the $N = 28$ gap. The same situation is expected to occur for the $N = 50$ and $N = 82$ shell gap below ^{78}Ni and ^{132}Sn, respectively. The reduction of the $N = 82$ gap would have extremely important consequences for the r-process nucleosynthesis.
- When reaching the neutron drip-line, proton-neutron forces may be weakened by the fact that neutrons are no longer confined in the nuclear potential well. The study of ^{26}F was proposed to test such effects. It was found that both the monopole and the residual proton-neutron interactions are weakened close to the drip-line as compared to the values used for nuclei close to stability. This very preliminary study is foreseen to be a benchmarking case for shell-model approaches or coupled cluster models which treat the influence of the continuum.

More generally, in the present work we have explored in a semi-quantitative manner several facets of the nuclear force which lead to modification of shell structure far from stability. Most of these properties were derived from two-body effective interactions (including monopoles) in the shell-model framework. The *effective* interactions are built from realistic bare interactions to which medium effects are added. These interactions are subsequently fitted to experimental data to include effects from missing terms such as the three-body components. The search for which parts of the nuclear interaction give rise to significant shell modifications was started a long time ago (e.g. in [112, 113, 114]). However very recent works manage to point out which properties of the bare nuclear force are preserved in the nucleus and which are modified. To quote a few it was found in Refs. [31, 70] that the tensor force is almost kept constant from the bare forces to the nucleus, while the central part of the interaction varies a lot. Moreover some theoretical works can now model nuclear systems with few nucleons or close to a core nucleus starting from realistic interactions or/and treat the interaction with the continuum.

As for experiments, important results are to come soon in the $N = 28$ region, such as the B(E2) value and the identification of higher-lying states in ^{42}Si, as well as the spectroscopy of neutron-rich Mg isotopes when approaching $N = 28$. Tremendous progresses have been achieved over the last 20 years since the first suggestion that the ^{44}S nucleus was deformed, based on its very short lifetime and small neutron delayed

emission probability [115], to the generalization of nuclear properties in all SO magic nuclei. All this was possible with the increase of experimental capabilities as well as regular exchanges between experimentalists and theoreticians.

7.1. Acknowledgments

J.-C. Thomas and R. Kanungo are greatly acknowledged for their suggestions and supports as well as for the careful reading of the manuscript. Discussions with F. Nowacki and T. Otsuka were essential for writing the parts of the manuscript related to shell model calculations and monopole decompositions. They are greatly acknowledged for this.

References

[1] Goeppert-Mayer M 1949 *Phys. Rev.* **75** 1969
[2] Haxel O , Jensen J.H.D. and Suess H.E. 1949 *Phys. Rev.* **75** 1766
[3] Sorlin O and Porquet M-G 2008 *Prog. Part. Nucl. Phys.* **61** 602
[4] Jurado B *et al* 2007 *Phys. Lett. B.* **649** 43
[5] Audi G and Meng W 2011 Private Communication, http://amdc.in2p3.fr/masstables/AmeFuture/mass.mas114
[6] Raman S , Nestor C.W. and P. Tikkanen 2001 *At. Data Nucl. Data Tables* **78** 1
[7] Liang X *et al* 2003 *Phys. Rev. C* **67** 024302
[8] Campbell PM *et al* 2006 *Phys. Rev. Lett.* **97** 112501
[9] Bastin B *et al* 2007 *Phys. Rev. Lett.* **99** 022503
[10] Winger JA *et al* 2001 *Phys. Rev. C* **64** 064318
[11] Gade A *et al* 2009 *Phys. Rev. Lett.* **102** 182502
[12] Zielinska M *et al* 2009 *Phys. Rev. C* **80** 014317
[13] Gade A *et al* 2003 *Phys. Rev C* **68** 014302
[14] Mengoni D *et al* 2010 *Phys. Rev. C* **82** 024308
[15] Bhattacharyya S *et al* 2008 *Phys. Rev. Lett.* **101** 032501
[16] Kanungo R 2012 contribution to the present volume.
[17] Dombràdi Z *et al* 2003 *Nucl. Phys. A* **727** 195
[18] Li ZP *et al* 2011 *Phys. Rev. C* **84** 054304
[19] Nowacki F and Poves A 2009 *Phys. Rev. C* **79** 014310
[20] Winkler R *et al* 2012 *Phys. Rev. Lett.* **108** 182501
[21] Glasmacher T *et al* 1997 *Phys. Lett. B* **395** 163 and references therein
[22] Force C *et al* 2010 *Phys. Rev. Lett.* **105** 102501
[23] Santiago-Gonzalez D *et al* 2011 *Phys. Rev. C* **83** 061305
[24] Cáceres L *et al* 2012 *Phys. Rev. C* **85** 024311
[25] Péru S *et al* 2000 *Eur. Phys. J. A* **9** 35
[26] Rodríguez-Guzmán R, Egido J.L. and Robledo M. 2002 *Phys. Rev. C* **65** 024304
[27] Ibbotson RW *et al* 1998 *Phys. Rev. Lett.* **80** 2081
[28] Nowacki F private communication
[29] Otsuka T 2012 contribution to the present volume
[30] Otsuka T *et al* 2005 *Phys. Rev. Lett.* **95** 232502
[31] Otsuka T *et al* 2010 *Phys. Rev. Lett.* **104** 012501
[32] Smirnova NA *et al* 2010 *Phys. Lett. B* **686** 109
[33] Takeuchi S *et al* 2012 arXiv [nucl-ex] 1207.6191
[34] Baumann T *et al* 2007 *Nature* **449** 1022
[35] Erler J *et al* 2012 *Nature* **486** 509.

[36] Cottle PD and Kemper K.W. 1998 *Phys. Rev. C* **58** 3761
[37] Nummela S *et al* 2001 *Phys. Rev. C* **63** 044316
[38] Sorlin O *et al* 2004 *Eur. Phys. J. A* **22** 173
[39] Gade A *et al* 2006 *Phys. Rev. C* **74** 034322
[40] Dechargé J and Gogny D 1980 *Phys. Rev. C* **21** 1568;
[41] Berger J-F , Girod M and Gogny D 1991 *Comp. Phys. Commun.* **63** 365
[42] Khan S *et al* 1985 *Phys. Lett. B* **156** 155
[43] Riley LA *et al* 2008 *Phys. Rev. C* **78** 011303
[44] Utsuno Y *et al* 2007 *Eur. Phys. J. Special Topics* **150** 187
[45] Gaudefroy L *et al* 2008 *Phys. Rev. C* **78** 034307
[46] Gaudefroy L 2010 *Phys. Rev. C* **81** 064329
[47] Gade A *et al* 2005 *Phys. Rev. C* **71** 051301
[48] Sarazin F *et al* 2000 *Phys. Rev. Lett.* **84** 5062
[49] Gaudefroy L *et al* 2009 *Phys. Rev. Lett.* **102** 092501
[50] Chevrier R *et al* 2012 *Phys. Rev. Lett.* **108** 162501
[51] Riley LA *et al* 2009 *Phys. Rev. C* **80** 037305
[52] Sohler D *et al* 2011 *Phys. Lett. B* **703** 417
[53] Riley LA *et al* 2009 *Phys. Rev. C* **79** 051303
[54] De Rydt M *et al* 2010 *Phys. Rev. C* **81** 034308
[55] Gaudefroy L *et al* 2006 *Phys. Rev. Lett.* **97** 092501
[56] Gaudefroy L *et al* 2007 *Phys. Rev. Lett.* **99** 099202
[57] Abegg R *et al* 1978 *Nucl. Phys. A* **303** 121
[58] Uozumi Y *et al* 1994 *Nucl. Phys. A* **576** 123
[59] Uozumi Y *et al* 1994 *Phys. Rev. C* **50** 263
[60] Holt JD *et al* 2012 *J. Phys. G.* **39** 085111
[61] Hagen G *et al* 2012 *Phys. Rev. Lett.* **109** 032502
[62] Zuker AP 2003 *Phys. Rev. Lett.* **90** 042502
[63] Moukaddam M *et al* 2011 *Acta Phys. Polonica B* **42** 541
[64] Porquet M-G and Sorlin O 2012 *Phys. Rev. C* **85** 014307
[65] Sieja K and Nowacki F 2012 *Phys. Rev. C* **85** 051301
[66] Bender M, P-H Heenen and P-G Reinhard 2003 *Rev. Mod. Phys.* **75** 121
[67] Sarkar S and Saha Sarkar M. 2010 *Phys. Rev. C* **81** 064328
[68] Hoff P *et al* 1996 *Phys. Rev. Lett.* **73** 2413
[69] Jones KL *et al* 2010 *Nature* **465** 454
[70] Smirnova NA *et al* 2012 *Phys. Rev. C* **86** 034314
[71] Eckle G *et al* 1989 *Nucl. Phys. A* **491** 205
[72] Burgunder G 2011 *PhD thesis* Université de Caen, France
[73] Nowacki F 2012 private communication
[74] Grasso M *et al* 2009 *Phys. Rev. C* **79** 034318
[75] Ebran J-P 2012 private communication
[76] Ring P 1996 *Prog. in Part. and Nucl. Phys.* **37** 193
[77] Sharma M M *et al* 1995 *Phys. Rev. Lett.* **74** 3744
[78] Lalazissis G.A *et al* 1998 *Phys. Lett. B* **418** 7
[79] Reinhard P.-G and Flocard H 1995 *Nucl. Phys. A* **584** 467
[80] Bender M *et al* 1999 *Phys. Rev. C* **60** 034304
[81] Bender M, Nazarewicz W and P-G Reinhard 2001 *Phys. Lett. B* **515** 42
[82] Pfeiffer B *et al* 2001 *Nucl. Phys. A* **693** 282
[83] Stanoiu M *et al* 2008 *Phys. Rev. C* **78** 034315
[84] Stanoiu M *et al* 2004 *Phys. Rev. C* **69** 034312
[85] Fogelberg B *et al* 1994 *Phys. Rev. Lett.* **77** 1020
[86] Jones K 2012 contribution to the present volume

[87] Fogelberg B *et al* 2004 *Phys Rev C* **70** 034312
[88] Tarasov O. B *et al* 1987 *Phys.Rev. C* **85** 011302
[89] Hoffman CR *et al* 2008 *Phys. Rev. Lett.* **100** 152502
[90] Kanungo R , Tanihata I and Ozawa A 2002 *Phys. Lett. B* **528** 58
[91] Hoffman CR *et al* 2009 *Phys. Lett. B* **672** 17
[92] Tshoo K *et al* 2012 *Phys. Rev. Lett.* **109** 022501
[93] Dobaczewski J *et al* 1994 *Phys. Rev. Lett.* **72** 981
[94] Catford WN *et al* 2010 *Phys. Rev. Lett.* **104** 192501
[95] Brown SM *et al* 2012 *Phys.Rev. C* **36** 765
[96] Obertelli A *et al* 2006 *Phys. Lett. B* **633** 33
[97] Terry JR *et al* 2006 *Phys. Lett. B* **640** 86
[98] Baumann P *et al* 1987 *Phys. Rev. C* **36** 765
[99] Nakamura T *et al* 2010 *Phys. Rev. Lett.* **103** 262501 and contribution to the present volume.
[100] Minomo K *et al* 2012 *Phys. Rev. Lett.* **108** 052503
[101] Wimmer K *et al* 2010 *Phys. Rev. Lett.* **105** 252501
[102] Utsuno Y *et al* 1999 *Phys. Rev. C* **60** 054315
[103] Hjorth-Jensen M 2012 contribution to the present volume
[104] Dobaczewski J, Michel N, Nazarewicz, Plozajczak M and Rotureau J 2007 *Prog. Part. Nucl. Phys.* **59** 432 and references therein
[105] Christian G *et al* 2012 *Phys. Rev. Lett.* **108** 032501
[106] Gaudefroy L *et al* 2012 *Phys. Rev. Lett.* in press
[107] Reed AT *et al* 1999 *Phys. Rev. C* **60** 024311
[108] Stanoiu M *et al* 2012 *Phys.Rev. C* **85** 017303
[109] Frank N *et al* 2011 *Phys. Rev. C* **84** 037302
[110] Lepailleur A *et al* 2012 Phd thesis University of Caen, and to be submitted.
[111] Brown BA and Richter WA 2006 *Phys. Rev. C* **74** 034315
[112] Talmi I and Unna I 1960 *Phys. Rev. Lett.* **4** 469; Talmi I 1962 *Rev. Mod. Phys.* **34** 704
[113] Poves A and Zuker AP 1981 *Phys. Rep.* **70** 235
[114] Federman P and Pittel S 1979 *Phys. Rev. C* **20** 820
[115] Sorlin O *et al* 1993 *Phys. Rev. C* **47** 2941